UTRECHT UNIVERSITY

FACULTY OF SCIENCE

Synthesis, passivation and characterization of lead-selenide supercrystals

Author:
Paolo ACCORDINI

Supervisors:
Prof. Daniël VANMAEKELBERGH
Dr. Ingmar SWART
Jaco GEUCHIES
Carlo VAN OVERBEEK

July 19, 2016

Abstract

Self-assembly and oriented attachment are used to build complex nanostructured materials. To characterized them, experimental techniques such as Scanning Tunnel Microscopy have to probe their surface, which is currently not feasible due to a layer of organic molecules that coat the entire volume of these materials. In this work, PbSe supercrystals were synthesized and ligand exchange techniques described in literature were adapted to remove the aformentioned organic layer. This would allow these superstructures to be probed under STM, while keeping the geometry and the electrical properties of these nanomaterials essentially unchanged. Two methods were developed and tested with varying degrees of success. The methodology was also extended to cover different types of nanomaterials, such as nanoplatelets.

Contents

List of Abbreviations

AFM	Atomic force microscopy
ALD	Atomic layer deposition
cALD	Colloidal atomic layer deposition
DySA	Dynamical self-assembly
FTIR	Fourier transform infrared spectroscopy
HOPG	Highly ordered pyrolitic graphite
NC	Nanocrystal
NMR	Nuclear magnetic resonance
NP	Nanoparticle
QD	Quantum dot
SA	Self-assembly
SC	Supercrystal
SL	Superlattice
SSA	Static self-assembly
STM	Scanning tunnelling microscopy
TEM	Transmission electron microscopy

Chapter 1

Introduction

Top-down approaches such as lithography, altough very precise, are very expensive and require special equipment. Bottom-up approaches, such as self-assembly, can be also used to assemble nanostructured materials, altough with some limits. Nonetheless these approaches have become one of the method of choice for exploring novel structures at the nanoscale, due to their low cost and relatively easiness.

In this thesis, a specific class of self-assembled structures was studied: PbSe supercrystals. In the synthesis of these materials, obtained through a solvent drying method, quantum dots were spontaneously brought together and fused into a large, atomically coherent crystal. Different geometries were observed, altough the most interesting one was the one colloquially called *honeycomb*: these structures are characterized by an honeycomb-like structure and they are not planar, making them similar to silicene.

The calculated electronic structure of these materials, showed that these structure are characterized by the presence of Dirac cones and other effects that stem from the strong spin-spin interaction found in these materials. However these theoretical predictions are lacking of an experimental confirmation. Scanning Tunnelling Microscopy (STM) could be used to confirm these predictions, but the surface of these supercrystals is covered with organic chains in constant thermal agitation, making the surface of these nanostructures practically not accessible to this experimenal technique.

In this work, a new protocol for removing ligands from the surface of supercrystals was developed by leveraging existing ligand exchange techniques used in literature. Oleic acid was displaced from the surface by a compact halide-based inorganic ligand, which resulted in the deposition of one atom thick halide layer on the surface. This not only should result in a greatly reduced thermal noise, but also the added layer bestows the supercrystal with great resistance from oxidation under ambient conditions. Finally, colloidal stability is retained by the formation of a double electrical layer.

Two delivery methodologies were developed, tested and compared. Transmission electron microscope (TEM) images confirm that the geometry is preserved at nanoscale, while the lack of specific peaks in the IR spectrum gathered with Fourier transform infrared spectroscopy (FTIR) hinted to a successfull removal of oleic acid from the surface.

Chapter 2

Theory

In this chapter, a brief overview of the concepts encountered during this work will be presented. The exposition will not be exhaustive, since a very broad range of topics were touched: basic colloidal chemistry, solid state physics, self-assembled systems and surface science to name a few.

section 2.1 will deal with quantum dots, giving a short introduction about nucleation theory and a brief overview on methods that are used in order to synthesize PbSe nanoparticles (NPs). section 2.2 will introduce the broad topic covered in this work, followed by a general introduction to self-assembly in section 2.3. Colloidal crystallisation will be introduce in section 2.4 and a focus on supercrystals will be given in section 2.5. Finally, section 2.6 will deal with the exact system investigated here. section 2.7 will deal with electronic properties in nanocrystals (NCs) and nanosolids such as the supercrystals (SCs) used in this work. The final section, section 2.8, will be devoted to a brief introduction to ligand exchange and how it is applied to superstructures.

2.1 Quantum dots

Quantum dots (QD) are nanometric crystals characterized by size-dependent photo-electrical properties. Initially these structures were synthesized on a suitable substrate using molecular beam epitaxy. Then, developments in chemical synthesis allowed the production of these nanocrystals using batch methods, thus enabling the study of colloidal QDs.

These nanocrystals are composed of an inorganic core made of a semiconductor material, such as PbSe or CdSe, and surrounded by an organic layer that provides the necessary steric stabilization and solubility in apolar enviroments. A 3D model is visible in Figure 2.1.

Due to their small dimensions (1-10 nm), these materials behave very differently from their bulk counterparts. The large surface-to-volume ratio implies that, contrary to what it is possible to find in macroscopical system, a significant fraction of atoms reside on the surface of the nanocrystals thus making surface contributions the most important ones. For example, larger surface areas contain more atoms and thus an higher amount of dangling bonds, which result in the destabilization of the overall nanocrystal.

This small volume affects also optical properties of these nanocrystals. Called *quantum confinement effects*, these properties start to emerge when the diameter of the nanoparticle is comparable to the Bohr radius of the bulk exciton. As the diameter of the NP approaches this

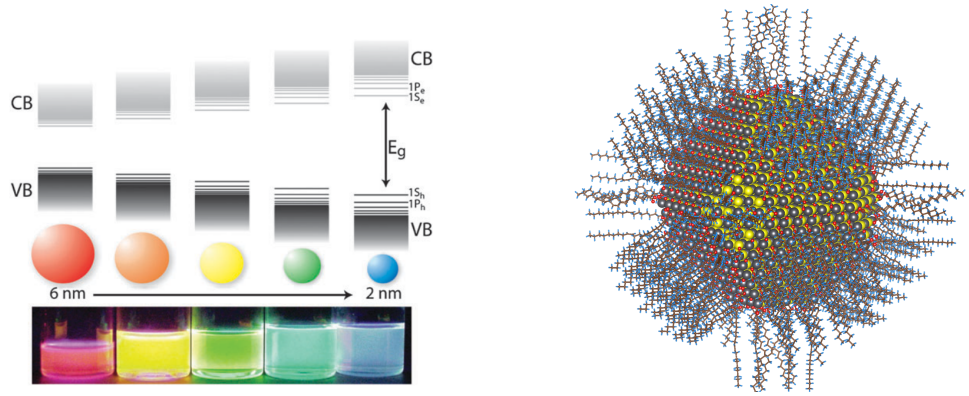

a b

Figure 2.1: ***Quantum dots and confinement-effects*** *- **a** Bandgap is increased as the average dot diameter is decreased. Formation of discrete energy states at the band edges is also visible. Reprinted from De Mello Donegá [1] - **b** 3D model of a PbS quantum dot, where it is possible to see the inorganic core, which stabilizes the nanocrystals in solution, that covers the nanocrystal.*

length scale, as shown in Figure 2.1, electrons and holes envelope wavefunctions are squezed in a small volume and they are forced to interact: these interactions increase as the diameter of the NC is reduced, resulting in a reciprocal repulsion that widen the bandgap between valence and conduction states. Thus, smaller particles have a larger bandgap than the bigger ones. Because of this, optoelectronic properties of these nanocrystal become size and shape dependent and they can be tuned at synthesis time.

2.1.1 Classical nucleation theory

Classical nucleation theory can be used to get a qualitative picture of the synthesis process. The formation of a nanocrystal can be described in three stages: induction, nucleation and growth.

Induction

During induction, no stable nuclei are formed and it involves a chain of reactions that lead to the formation of subcritical clusters of monomers. The cluster grow until a critical radius r_c is reached.

Nucleation

At this point, the nucleation phase starts. Formation of a new stable nuclei will happen only if the energy of the system is lowered in the process. The Gibbs free energy for the formation of a stable nuclei of radius r is:

$$\Delta G = \Delta G_v + \Delta G_s = \frac{4}{3}\pi r^3 \rho \Delta\mu - 4\pi r^2 \gamma \qquad (2.1)$$

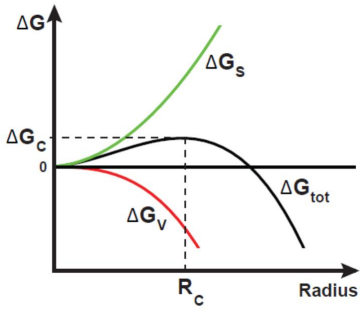

Figure 2.2: ***Plot of formation energies****: Surface (green) and volume (red) contributions to the total Gibbs free energy. The two terms cancel out at the critical radius r_c, meaning that nuclei bigger than the critical radius will tend to grow whereas the smaller ones will tend to dissolve. Reprinted from Joep [2]*

where r is the radius of the nuclei, ρ is density, $\Delta\mu$ is the difference in term of chemical potential between the bulk phase and the free monomers for the material that the nuclei is composed of, γ is the interfacial energy. Formation energy can be understood in terms of a volume term, ΔG_v, and a surface term, ΔG_s. The former one, related to the addition of monomers to the original nuclei and thus the formation of new surface bonds, is always negative. The latter, is related to surface tension and it is always positive, because the creation of surface always requires energy.

From ΔG, shown in Figure 2.2, it is possible to understand how the system will behave. By taking the derivative with respect to r an setting it to zero it is possible to find the critical radius r_c:

$$r_c = \frac{2\gamma}{\rho\Delta\mu} \tag{2.2}$$

where $\Delta\mu = -k_b T \ln[x/x_{sat}]$, T is the temperature, k_b is the Boltzmann constant and x/x_{sat} is the degree of saturation. The dependency of the critical radius from the temperature suggests that bigger/smaller nuclei can be obtained by reducing/increasing the temperature and by reducing/increasing the degree of supersaturation. Nucleation rates are also affected by surfactants: if precursor reactivity is enhanced by the surfactant, the nucleation rate is increased and the converse is also true. But surfactants also play a role in coordinating the monomer species, where a higher concentration of surfactants will lower $\Delta\mu$, thus increasing r_c. The nucleation event ends when the temperature drops below the nucleation temperature or when the concentration of monomers in solution drops below the saturation threshold.

Growth

Growth of a nanoparticle can happen in two ways: incorporation of monomers from solution or coalescence of two particles into one. In the first route, a monomer in solution diffuses toward the surface of the nuclei and gets incorporated. In the second case, two particles gets fused together, surface gets reconstructed in order to minimize its surface energy and in this process the particle usually become more spherical. Both ways happens at the same time during this phase: however, the final size of the nanoparticles during this process is roughly the same.

The monomer concentration can deeply affect how the growth may proceed. At low concentration, the rate limiting step in the monomer addition reaction is due to the time needed for the monomer to reach the nanoparticle. This regime is called *diffusion limited*. However, at high monomer concentration, the diffusion is so fast that the diffusion process can be neglected. This regime is called *reaction limited*. The advantage of the reaction regime is that smaller nanoparticles will grow faster than the bigger ones, leading to a focusing of the size distribution.

The growth is also modulated by the capping ligands, as they can control the growth by steric hindrance. In particular, higher binding energies between nanocrystal and ligand will results in a smaller crystal, whereas losely bounded ligands will promote growth of the nanoparticle.

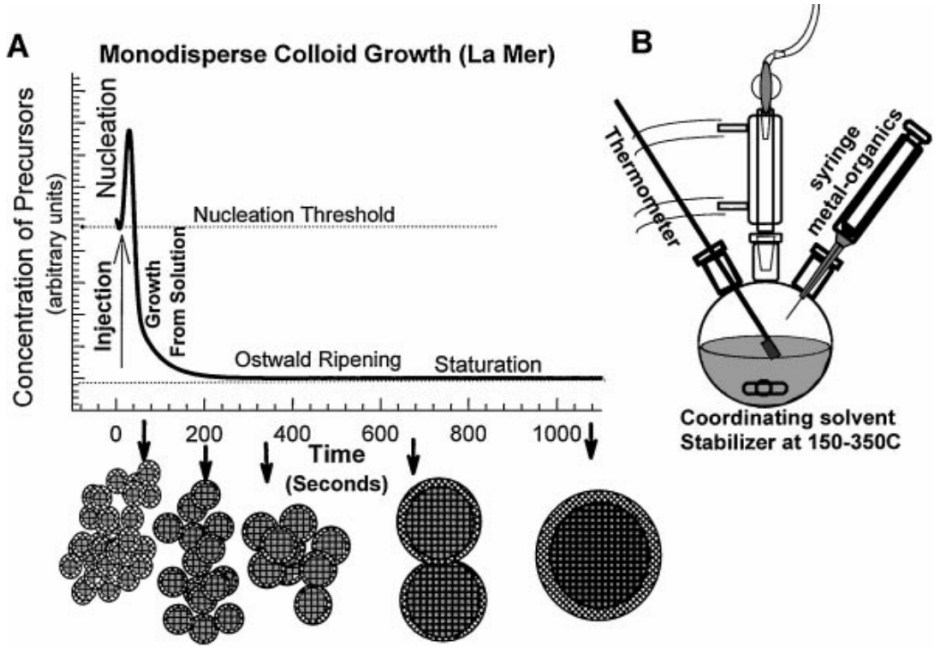

Figure 2.3: ***Hot injection method****: **a** - Concentration versus time graph of a generic hot-injection reaction. five distinct phases are showed under the time axis. From left to right: nucleation events, right after the injection of the cold precursor. Growth continues until the beginning of the coalescence of nanoparticles due to Ostwald ripening.* ***b*** *- Depiction of the usual experimental setup employed for hot-injections. The three necked flask contains one of the precursor, which is heated up to high temperatures, such as* $180\,^{\circ}\mathrm{C}$ *in the case of PbSe nanoparticles. A reflux column is attached to the system, in order the recondensation of the organic solvents and to add extra expansion volume for the nucleation burst. Finally, a syringe with the cold precursor is attached on the third sealed neck. Reprinted from Murray et al* [3] *.*

2.1.2 Synthesis

Classical nucleation theory, altough useful as a first approximation, makes some assumptions that are not observed in real case scenarios. For example, surface tension γ is assumed constant for the whole reaction whereas the value of this parameter can change for different crystal facets, which they will have different growth rates, and hence sizes and surfaces, during the growth process.

A synthesis method that is qualitively described by the classical nucleation theory is the hot injection method, shown in Figure 2.3. First developed by Murray [3] , it is used nowadays in most of the syntheses related to semiconductor quantum dots. Strong points of this method are the ability of obtaining nanocrystals with a low degre of polydispersity ($\leq 5\%$ nm) and high quantum yields (85%).

A typical synthesis begin with the preparation of two precursors: the metal one, dissolved in an organic solvent and the chalcogenide one, dissolved in a coordinating agent. The first precursor is usually composed of an metal-ligand complex with excess ligands in an apolar solvent with a high boiling point.

These syntheses are characterized by the presence of two steps: the first one involves heating up the first precursor to a defined temperature, for example this temperature is equal to $180\,^{\circ}\mathrm{C}$ when dealing with PbSe quantum dots. The second one involves the rapid injection of the other precursor kept a room temperature. This step induces a condition of supersaturation

in the solution, causing nanoparticles to nucleate. This method ensure the synthesis of a narrow size distribution because after the injection the concentration of monomers in solution is decreased significantly and no new nuclei can be formed.

The average size distribution is determined by the time given to the particles to consume monomers in solution. When the required time for the growth stage is finished, temperature is quenched rapidly. This is done in order to prevent an effect called *Ostwald ripening*, which promotes the dissolution of smaller nanoparticles to allow the growth of bigger ones causing an undesired broadening of the size distribution.

The final product is precipitated through the addition of excess anti-solvent and NPs are centrifugated, decanted and redispersed in an apolar organic solvent such as toluene or hexane. These steps are repeated two or more times, depending on the degree of purification needed. This also depends on the nature of the anti-solvent: for example, many cycles with methanol may result in a loss of colloidal stability due to its ability to cleave oleic acid molecules from the surface of the nanocrystal whereas acetonitrile does not have this effect since it does not interact appreciably with the organic layer [4] .

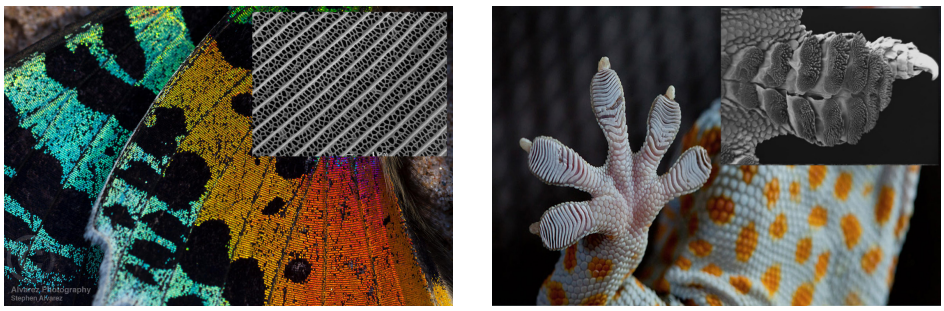

a **b**

Figure 2.4: ***Examples of nanomaterials in nature*** *- **a**: a butterfly wings. Inset shows a magnified version of a typical butterfly wing, where it is possible to see the microstructures that allow light to bounce in a way that generates the colorful patterns visible with the naked eye. From a material science point of view, these microstructures are an example of a photonic crystal, a structure that can be used to manipulate and steer light. **b**: a gecko paw. Inset shows the microscopic structure of the paw, where its surface is composed of many microscopic pillars. Gecko's ability to stick on any surface is given by the attractive forces given by the sum of all Van der Waals interactions induced by these pillars and the surface.*

2.2 Nanomaterials

Nanomaterials are characterized by a defined structure at the *nanoscale*: in other words materials with individual features in the range of 1-1000 nm. This definition put strict requirements on the level of precision needed in order to allow a material to be classified as such. The whole spectrum of techniques used to produce these materials can be divided in two broad classes: the *top-down* and *bottom-up* approaches.

This terminology is used to encode the way these approaches tackle the problem of the production of nano scale objects and materials. In the top-down case, macroscopic machines (the *top*) are used to pattern and create nanometric features (the *down*). On the other hand, bottom-up techniques use the opposite route, starting from nanoscopic building blocks (the *bottom*) to build complex structures that can goes beyond the nanoscale (the up).

Micro and nano fabbrication methods such as lithography, but also thin film deposition techniques such as atomic layer deposition (ALD), can be used to produde system that are characterized by nanoscale features. In particular, these technique can be used to mass produce large scale atomically precise object. Probably the most famous example of this methodology are the microprocessors found in a common desktop computer, where features as small as 14 nm are routinely carved using beam lithography.

On the other hand, bottom-up methods work in the opposite way: complex structures and material are autonomously assembled from nanoscopic building blocks (i.e. quantum dots, surfactants molecules, ...) by exploiting nature's tendency to minimize energy. This approach is commonly referred to *self-assembly*. These methods are used in biological systems to synthesize different and interesting materials that are still studied today for their complexity and possible applications. Some examples are visible in Figure 2.4.

The first method can be used to produce high precision materials but it can be done essentially in a serial way, usually under experimental conditions not readily accessible (i.e. clean chambers) and usually expensive machinery are needed. On the other hand, self-assembly can be used to produce materials with a lesser degree of precision, but the synthesis relies on heavily parallelized chemical processes and the experimental conditions necessary does not

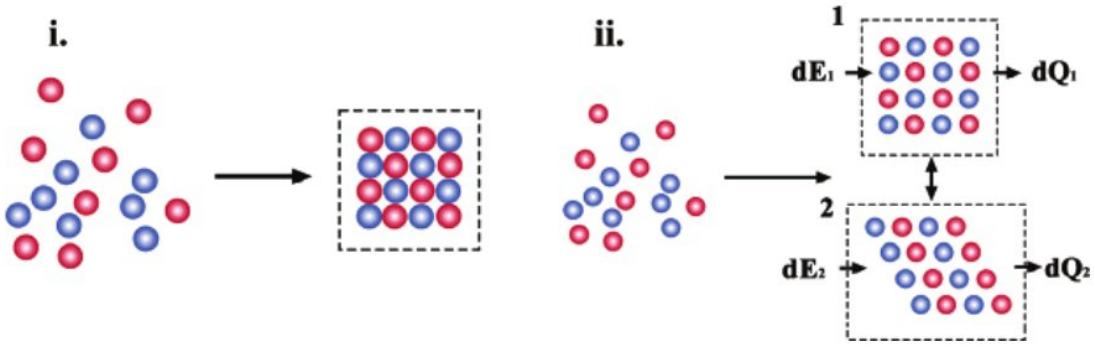

Figure 2.5: ***Dynamical self-assembly and Static self-assembly****: **i.** Schematic depiction of static self-assembly (SSA), where a configuration of elementary objects (left) start to interact and the system reach its equilibrium (right). Once the global (or local) minimum of energy is reached, the system stays in this configuration indefinetely. **ii.** Schematic depiction of dynamic self-assembly (DySA), where a generic system (left) can, depending on the condition, assume different nonequilibrium configurations. Represented as system 1 and 2 (right), these configurations require energy to mantain their local order, as highlighted by dE_1 and dE_2 in the rightmost picture. When the energy input is turned off, these systems are not able to keep their order anymore and the revert back to a disordered state. Reprinted from Fialkowski et al.* [5]

requires extremely expensive equipment: these last two feature are the ones that make these methods so compelling.

2.3 Self-assembly

This category can be further divided in two branches: *dynamic* and *static* self-assembly. The different between these two classes lies in their thermodynamical description [5] .

In the case of dynamical self-assembly (DySA) the system must be brought out of equilibrium first and, through a constant supply of energy, its building blocks interact and find another stable nonequilibrium configuration. In this process, energy is supplied to the system which is converted in a higher degree of local order by the emission of entropy in the surrounding environment. However, as soon as the energy input is stopped, the nonequilibrium state cannot be mantained anymore and the structure cease to exists.

This class of structures belong to a broad class of nonequilibrium steady-state systems that have been under intense study for many years, but they are still poorly understood due to different problems related the physical description of the systems: for example, in this regime entropy is not maximised which forbids a variational mathematical formulation and pose problems for its modelling [5] .

Before proceeding, self-assembly have to be defined in a more rigourous way. Using the word provided by Fialkowski et al. [5] :

> *We limit SA to the spontaneous formation of organized structures from many discrete components that interact with one another directly (e.g., electrostatic interactions between charged objects) and/or indirectly through their environment (e.g., chemotactic interactions between bacteria, which create and respond to chemical gradients in a surrounding medium). In addition, the assembling components may also be subject to*

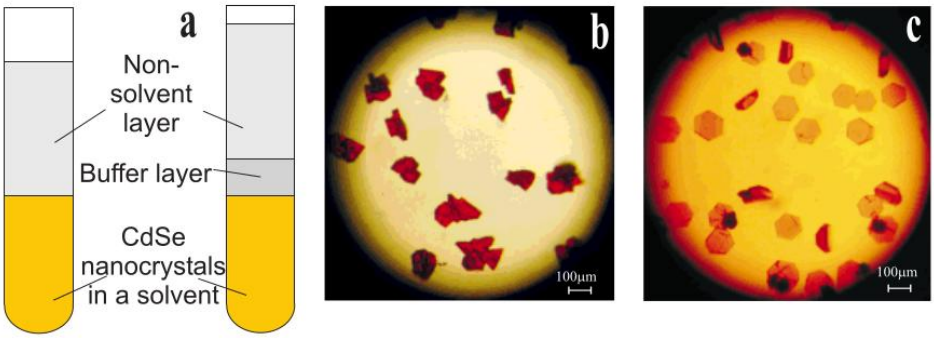

Figure 2.6: ***Close packed CdSe superlattice**: **a** - The two experimental systems explored by Talapin et al. Both vials were left undisturbed for two months. Both systems are composed of two immiscible phases: a concentrated CdSe quantum dot solution and a non-solvent phase. The buffer layer, composed of 2-propanol and present only in the rightmost vial, slows down the diffusion of the non-solvent in the quantum dot phase. This results in different rates of nucleation and higher quality of superlattices. Fast nucleation, obtained in the leftmost vial, is shown in figure **b** while slow nucleation, obtained in the rightmost vial, is shown in figure **c**. It is possible to see how well defined hexagonal shapes were obtained only in the second vial. Reprinted from Talapin et al [6] .*

> *various global (confining) potentials such as externally imposed electromagnetic fields or chemical gradients.*

Static self-assembly (SSA) relies on the minimization of its free energy, resulting in a stable configuration that correspond to a local or global energy minima for the system. The difference with the DySA case mentioned above, is that no constant influx of energy is needed in order to maintain the self-assembled configuration on the equilibrium configuration is reached.

2.4 Colloidal crystallisation and superlattices

From a broad thermodynamical point of view and assuming constant temperature and pressure, the formation of these structures is driven by the minimization of the Gibbs free energy of the system:

$$\Delta G_{sys} = \Delta H_{sys} - T\Delta S_{sys}$$

Where ΔH_{sys} contains energy contributions due to all the possible nanoparticle interactions, such as electrostatic interaction between coresΔS_{sys} contains the entropic contributions . The overall behaviour of the system is dictated by how these two factors interact. Two extreme cases can be identified: $\Delta H_{sys} = 0$ or $\Delta H_{sys} \gg T\Delta S_{sys}$.

In the first case, $\Delta H_{sys} = 0$ and the system is driven by the maximization of the entropy. This is usually the case described by a system of hard spheres. Since no interactions are present, system reaches its energy minimum by packing as

One class of materials that can be synthesized with SSA and it is relevant to the topic of this work is the synthesis of superlattices. In these materials, nanoparticles are the basic building blocks and these structure are referred as *superlattices*, since they share lots of properties such as periodicity and long range order with a normal atomic lattice. As crystals are long range

ordered dispositions of atoms, superlattice are long range ordered dispositions of colloidal nanoparticles.

An example of these system is shown in Figure 2.6. The underlying mechanism of formation is static self-assembly. By using CdSe nanoparticles, Talapin et al [6] managed to form a close packed configuration in two ways, altough both conceptually related. The controlled destabilization of the organic capping of the quantum dots cause a gradual loss of capping ligands, which in turn increases the interaction forces between quantum dots and bring them closer together. Eventually they form an ordered superlattice. Another similar experiment was prepared with an added immiscible phase, used to modulate the diffusion of the non-solvent in the phase that contained quantum dots. Altough both experiments used the same chemical mechanism, the second one was slower and thus promoting more ordered aggregations. This was clearly demonstrated by the images of the samples collected after two months of growth: both experiments showed superlattice configurations but, whereas dots in the second experiments formed hexagonal shaped flakes as large as $100\,\mu$m, the first experiment lacked the hexagonal structure. This was interpreted as the effect of too fast crystalization, compared to a much slower one.

It is worth noting that in these structures quantum dots are still disconnected from each other: they are *close*, but not connected. In other words, between every quantum dot that forms the lattice ligands are still present and they prevent the bare crystallographic planes of the ajacent quantum dots to come in contact and the respective atoms on the surface to form bonds.

One appealing feature that characterize these systems is that the dimensionality of the these lattices, i.e. a tri-dimensional structure or a bi-dimensional one, can be tuned as well by choosing the appropriate synthesis method. In the example shown above, nanocrystals are free to move in a volume of solvent, altough in weakly flocculated state. These degrees of freedom allow the nanoparticles to organize themselves in a 3D structures. However, by confining the system on a bidimensional surface, such as a an immiscible phase for the solvent, NPs can be forced to assume bidimensional configurations.

2.5 Supercrystals

Supercrystals are the closest relative to superlattices: they have no ligands in between their elementary building blocks, since nanocrystals are atomically fused along very specific facets. This result in the removal of any extra space that may deteriorate electrical performances. However, ligands are still present on the facets that were not used for self-assembly.

This difference between these two class of structures, superlattices and supercrystals, is achieved through a phenomena called *oriented attachment*, where under particular conditions an ensemble of weakly flocculated nanocrystals lower their surface energy by fusing along specific facets with neighbouring dots. The first experimental observation for this effect was described in a work done by Penn et al. [7] , where they described how TiO_2 nanocrystals were coarsensed by oriented attachment. The central idea of their finding was that the growth was promoted only along very specific crystallographic directions. In the following years many other examples of oriented attachment were found with different types of nanocrystals and used to synthesized interesting morphologies.

For example, Cho et al. [8] describes a way to synthesize nanowires by exploiting this effect. In their paper, nanowire long up to $30\,\mu$m are obtained by selectively attach quantum dots on

specific facets: oriented attachment happened mainly through the {100} facets, however they also noted that this could be changed. Addition of primary ammines allowed the attachment to use also the {110} facets.

There are *two* possible routes for which the attachment process [9] can take place. In the first one, two primary particles collide and if the two colliding planes are compatible, the fuse together in an irreversible process that produces an oriented aggregate. In the other mechanism, nanoparticles form a complex first, then they rotate into the right orientation and fuse together.

PbSe quantums dots can also be used to form complex structures through the exploitation of oriented attachment. In this research, two different morphologies were successfully synthesized using this method: superlattices with square and honeycomb geometries on the nanocrystal scale. The first type is a planar structure composed of quantum dots where, ideally, each one dot is attached with four other neighbouring nanocrystals, altough strain and other effects tend to deform this structure, thus inducing an angle between dots that is slightly less than 90 degrees. The second one is more interesting, because its geometry is similar, but not equal to, the one that defines graphene. The shape of the unit cell induces the formation of remarkable features in the electronic structure called Dirac cones, but also other interesting effects [10] , there is a lot of works on this particular types of structure.

However, little is known about the actual synthesis pathways behind these structures and more research is needed in order to uncover its secrets. In this section, a brief overview of what is currently accepted about the formation of these structures will be presented. Possible explanations for the most interesting points will also be given: however, due to the lack of experimental evidence, they have to be taken more as an “educated guesses”.

The pathway followed by quantum dots in order to form ordered superstructures can be divided in three stages: evaporation, formation of a close-packed configuration and the final oriented attachment. Honeycombs are special in this regard, since another stage may be required: buckling. All these stages will be covered below.

2.6 PbSe Supercrystal

In this work, PbSe quantum dots were employed to synthesize PbSe supercrystals. The dynamics behind the formation of these crystals are still poorly understood, but they can be divided in three phases, with a fourth one which is specific for a particular supercrystal conformation. The proposed mechanism is pictured in Figure 2.7.

Superstructures are synthesized starting by the spontaneous evaporation of a solution that contains PbSe quantum dots on top of an immiscible liquid phase, ethylene glycol. The protocol is sensitive to concentration [11] and thus differente concentration of quantum dots usually lead to different types of superstructures at the end of the synthesis. Solvent also plays a role [2,12] , where different organic solvents seems to lead to different outcomes.

As soon as the solution is dropcasted on top of the EG phase, the solvent first wets the surface and then it starts to evaporate. Experimentally it is known that the way that the solution evaporates affects the final superstructure. In particular, slow evaporation seems to favour square-like attachment.

Once the solvent is completely evaporated, quantum dots are diffusing on the liquid-gas interface. Calculations performed by Evers et al. [11] showed how quantum dots may be absorbed at the interface.

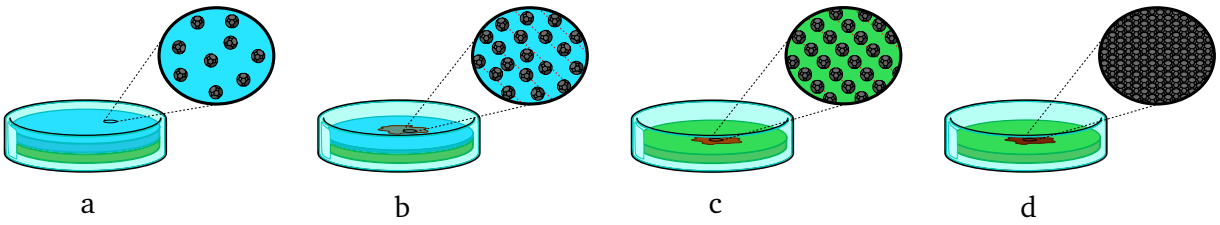

Figure 2.7: ***PbSe supercrystal self-assembly process*** *- from left to right: (**a**) quantum dots solution is dropcasted on top of an immiscible phase. The organic solvent starts to evaporates due to its high vapor pressure. (**b**) Near the end of this evaporative process, quantum dots start to interact thus forming the early stages of a close packed configuration. An initial brownish film can be seen on the liquid-gas interface. (**c**) Meanwhile, ethylene glycol is destabilizing the organic capping by gradually removing oleic acid molecules from the surface of the dots: this result in an increased interaction between the nanocrystals. (**d**) After about* 60 min*, quantum dots on the surface are connected along the {100} facets and form a coherent supercrystal.*

Simulations showed how the shape of the dots can deeply affect the way nanocrystals are absorbed on the interface and how large absorption energies are ($\approx 10^2 kT$). The depth of this potential well hints to an irriversible absorption at the surface, while the shape dependency defines if the dot will be absorbed only along the {100} facet or with a combinations of the other facets.

At a point in time, quantum dots on the surface will most likely start to be gradually destabilized by the loss of oleic acid molecules to the interface of the liquid phase. As time passes by, interactions will become more and more attractive due to the loss of steric stabilization and dots will be brought closer together.

This is the final stage of the synthesis, where the quantum dots align their crystal planes and form atomic bonds between {100} facets and they form a single crystal. This is the least understood step of the process, since to date there is no accepted mechanism able to explain how superstructures with a long range order can be formed from a configuration of close packed quantum dots in a weakly flocculated state.

One way to explain this superstructures can be traced back to dipole-dipole interaction. Talapin et al. [13] showed how these structures may be formed by the minimization of dipole-dipole interaction, but up to now the dipole moment of these nanocrystals has not been experimentally determined. Moreover, the model proposed by Cho et al. [8] for the origin of the dipole moment in NCs with a rock-salt lattice has not been verified experimentally [14] .

In the case of honeycomb supercrystals, there is another step in between the initial close packed configuration and oriented attachment, called *buckling*. This step was included in order to explain the observed periodic out-of-plane deformations of these superstructures. It is not clear how these deformations happen during the synthesis of these supercrystals, since there is no accepted mechanism that can push out of the plane quantum dots in such a precise and periodic way.

2.7 Electronic properties

As the electronic properties of a quantum dots arise from the interplay of confinement effects and its crystalline structure, a similar effect can be expected when dealing with many quantum dots coupled together in a ordered lattice.

The emergence of collective phenomenas in these systems is akin to what happens to the electronic structure inside a crystal. In the latter system, orbitals from individual atoms interact due to their proximity to each other and they split in multiple states. In the same way, collective wavefunction leaking out from a quantum dot can interact with the other quantum dots around, leading to the formation of continuous bands.

But there are some important differences between the formation of bands inside a crystal and inside a superlattice: whereas isolated atoms are identical in every sense, every quantum dot is different from each other. This is due to many factors like size, ligand coverage, composition type and so on. This dishomogeneity changes the overall envelope wavefunction and thus changing the way levels split.

First, interaction between *ideal* quantum dots will be analyzed, and then dishomogeneity effects such as the ones listed above will be introduced in the picture to see their effects.

Then, as the separation between two neighbouring ideal dots is reduced, their envelope wavefunctions can overlap leading to quantum mechanically coupled dots. The strength of the coupling has an exponential dependency on the spatial width (Δx) and square root of energetic height (ΔE_c) of the barrier between the dots. An approximate equation that describe this relation is [16] :

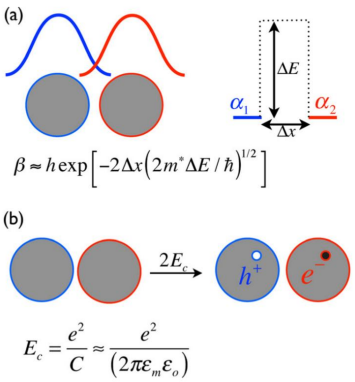

Figure 2.8: ***Coupling in quantum dots solids**: **a** Quantum mechanical coupling of two envelope wavefunction of two ideal spherical quantum dots interact and allow charges to be moved around. The coupling strength depends on the distance between the dots, but also on an energy barrier due to eletrostatic interaction. **b** The magnitude of this energy barrier is associated with the energy required to move one charge from one site to another, and depends both on the dielectric environment that surround the QD and the self-capacitance of the dot. Reprinted from Hanrath et al. [15]*

$$\beta/h \approx \exp\left[-2\Delta x\left(\frac{2m^*\Delta E_c}{\hbar}\right)^{1/2}\right] \tag{2.3}$$

where m^* is the effective mass of the charge, Δx is the spacing between dots and ΔE_c is the electrostatic energy required to move a charge from one dot to another. This last factor is related to the fact that moving a charge around, i.e. hopping from one dot to another, involves a Coulombic energy penalty. The magnitude of this penalty is connected to factors such as self-capacitance, which is connected not only to the size and shape of the dot, but also to the dielectric environment that surround the system. Approximatively, this penalty can be quantified by:

$$E_c = \frac{e^2}{C} \approx \frac{e^2}{2\pi\epsilon_m\epsilon_0} \tag{2.4}$$

As the coupling between atoms in a periodic lattice lead to the formation of bands in crystals, the coupling between ideal quantum in a periodic lattice form extendend states, called

minibands, separated by energy gaps. The number of states inside a miniband correspond to the number of dots in the crystal, while the magnitude of the gap between the bands is connected to the way dots are coupled together. Generally speaking, the bandwidth is proportional to the coupling energy and thus weak coupling lead to narrow bands and large gaps, whereas the opposite case will lead to wide bands and small gaps, as shown in Figure 2.9.

Simulations using Si/Ge models suggests that minibands can form for a separation gaps smaller than 2 nm. When *real* quantum dots are used in this picture, i.e. nanocrystals characterized by statistical fluctuations in size, shape and composition, etc., two situations can arise: localized or delocalized states can emerge. The discriminant between these two conditions is given by how strongly coupled the quantum dots are and the degree of dishomogeneity, which affects the energy levels distribution, denoted by $\Delta\alpha$.

In the case of strongly coupled, identical dots, $\beta > E_c$ and charges are free to hop from one site to another. In this case, so called extended states are formed, where the envelope wavefunction is spreaded among many dots. On the other hand, if energy level fluctuations, i.e. the broadening of the energy levels $\Delta\alpha$, are larger than the coupling energy then the cost to move charges around is too high and charges are trapped inside the quantum dot. In this case, the envelope wavefunction is confined in the quantum dot and localized states are formed instead.

This behaviour is connected with the problem of charge transport in disordered materials and it was addressed by Anderson [19] , who showed that after a certain degree of disorder, diffusion of charge will stop regardless of their ability to tunnel from one site to another.

Consequences of this effect can be detected not only from conductivity measurements, but also from the light absorption properties of the material. In particular, the absence of modification to the absorption spectra due to strong coupling found in CdSe superlattices from Murray et al. [20] was explained using this effect. Simulations done by Artemyev et al [21] showed how even in highly ordered structures, delocalized states and thus mini bands, are hardly noticeable even at very high packing fraction.

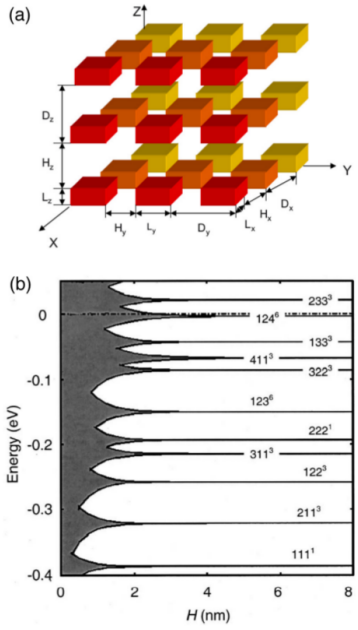

Figure 2.9: ***Miniband formation**: **a** - Schematic of the three-dimensionally ordered quantum dot superlattice showing notations for the quantum dot sizes and interdot spacing. **b** - Miniband width as a function of the interdot distance H. The size of the dots is L=6.5 nm. The important observation is that even the miniband, which lies above the barrier (E > 0), evolves to a discrete level as the interdot distance increases. Reprinted from Nika et al. [17] and Lazarenkova et al. [18]*

These results were also observed in this work, since absorption peaks were not changed noticeably by the coupling between dots, suggesting a certain degree of disorder on the surface. This makes sense since the morphology on the surface is usually characterized by different types of superstructures connected together.

2.7.1 PbSe supercrystal electronic properties

Electronic structure for these materials has yet to be determined experimentally. However, due to their novelty as a material and their interesting geometries, these properties were calculated using numerical methods.

The theoretical exploration of these structures was performed using tight binding calculations and different truncation parameters were employed, in order to highlight the shape-dependent effects on the electronic structure. In every case explored, both square and honeycomb lattices, effects observed were correlated with what authors called *nanogeometry*.

This term was coined in order to identify the periodic arrangements of holes in the planar structure, which are dependents on the size and shape of the building blocks used in the self-assembly process.

Square lattices were explored by Kalesaki et al. [22] , where they have determined the electronic structure of PbSe, CdSe and CdTe using tight-binding approximations. In this work, they have observed how the electronic structure of these planar two-dimensional superstructures showed an electronic structure that depart from the ones observed in genuine 2D semiconductors. In particular, they have observed that the electronic structure found in these lattices were not only influenced by the geometry of the lattice but also by the configuration of the holes formed by the quantum dots.

When CdSe supercrystals were considered, two lattices were compared: one formed by quantum dots with zero truncation, i.e. a flat 2D uniform semiconductor, and with a non-zero truncation, and thus with a periodic array of holes in the lattice. They have found that truncations induced periodic scattering of the electronic waves in the lattice, causing the opening of gaps at the center and at the edges of the superlattice Brillouin zone.

CdTe supercrystals electronic structure resemble the one found for CdSe, altough the strong spin-orbit coupling induce considerable spin-splitting in both the valence and the conduction bands. In the paper, it was noted that such large spin splittings are not due to the nanogeometry, and similar effects were also found in CdTe quantum wells.

In case of PbSe, it was found that the overall behaviour is similar to what was found in the case of CdSe, however the PbSe superlattice bands showed more hybridization. The splitting indicates that the energy and coupling of NC wave functions are not only defined by the symmetry of the envelope function but also by the underlying Bloch function which depends on the originating valley. Other works in literature predict that, when using no truncation and thus when quantum dots form an uniform 2D monolayer, results compatible for topological insulator states could be found [23] .

Kalesaki et al. [10] also explored the eletronic structure of honeycomb superlattices. However, in their work, they used the {110} and {111} facets as possible way to attach the nanocrystals: recent work showed that this is not the case and the {100} facets are indeed used for epitaxial attachment.

A similar work was carried out for HgTe honeycomb superlattices [24] , where it was shown how this novel material, due to the strong orbit coupling of HgTe combined with the honeycomb structure results in several topological phases.

2.8 Ligand exchange

Ligand exchange is a chemical procedure where colloidal system, usually sterically stabilized by organic chains absorbed on the surface of the system, can be exchanged for different ligands in order to obtain different results. To name a few, this technique can be used to obtain functionalization, better electronic coupling or to increase stability under ambient conditions.

In order to understand how ligand exchange has to be performed, a deeper knowledge of how these molecules are absorbed on the surface of the nanostructure is needed. In literature it is possible to find works that describe the surface chemistry of CdSe and PbS quantum dots: however the amount of papers on PbSe nanocrystals is very small in comparison. Since surface chemistries of PbS and PbSe NC are similar, many of the assumptions made in this work are based on the former type of quantum dot.

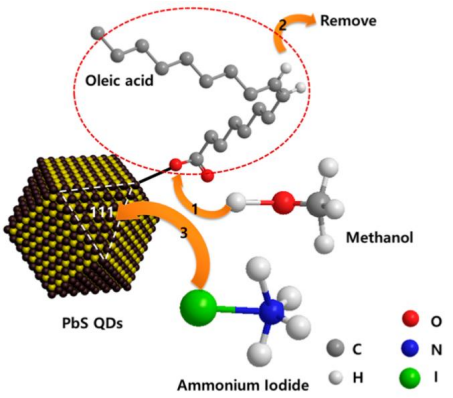

Figure 2.10: ***Ligand exchange scheme****: Schematic depiction of the ligand exchange process assumed in this work. In this process, short alchohols such as methanol can cleave the bond between OA and the QD, exposing the underlying {111} surfaces. The new ligand donates the halide ion to a Pb ion. The NH_4^+ cation neutralize the charge by forming an electrical double layer. Reprinted from Kim et al.* [25]

In the case of PbSe quantum dots, the exchange dynamics can be explained through the HSAB principle (Hard and Soft Acid and Bases). This qualitative principle is used to explain the stability of compounds and reaction mechanism. In this context, *hard* is applied to small, weakly polarizable and with an high charge state chemical species. *Soft* is applied to big, highly polarizable and with low charge state chemical species. Qualitatively, the theory predict that *soft acid* will react preferably with *soft bases* and *hard acid* will react with *hard bases*.

Accordingly to this principle, Pb^{2+} is a soft acid. Halides, which are Lewis bases, bond in the following order, going from the most basic to the most acidic ones: $I^- > Br^- > Cl^- > F^-$.

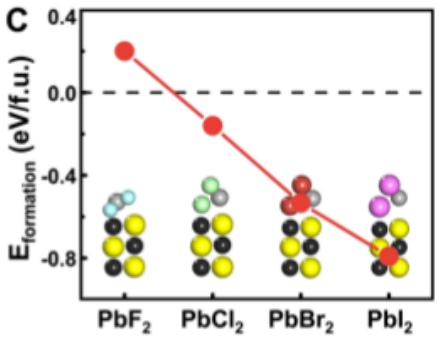

Figure 2.11: ***PbX_2 formation energies****: DFT formation energy of various PbX_2 adlayers on the PbSe(100) surface. Negative formation energies are predicted for all halides, except fluorine. Reprinted from Kim et al.* [25]

Fluorine, due to its small radius and low polarizability is a hard base, while iodine with its larger ionic radius and high degree of polarizability, can be understood as a soft base. The strongest bond should be formed by Pb^{2+} and I^- while fluorine, being an hard base, should not be able to form a stable layer, as confirmed by DFT calculations [26]. Results for the aforementioned theoretical calculations are visible in Figure 2.11.

Works in literature [27,28] suggest that most of the passivating ligands are absorbed on {111} surfaces. Protic, or organic solvents with a labile H^+ atom, are amines or short-chain alcohols, such as methanol, that can etch surface atoms terminated by carboxylate ligands. This result in exposed {111} surfaces that, due to the higher affinity between I^- and Pb^{2+}, are terminated by Iodide. Thanks to the formation of an atom-think layer of Iodide on the surface, oxygen cannot bind to Pb, thus prevent-

ing the formation of stable lead-oxygen compounds that lead to colloidal destabilization and degradation of the optical properties. This mechanism was tested with all halides, resulting in quantum dots that are stable under ambient conditions for weeks [26] , with the only exception of fluorine.

Among other possible uses, in literature ligand exchange techniques are employed as an efficient way to swap the native ligand for a shorter one. By decreasing the length, the interparticle distance is reduced. This change in inter-nanoparticle distance has impact on many properties of ordered quantum dot assemblies, since electronic properties such as current conduction are strongly dependent on the rate of electron hopping from dot to dot. Because this rate is dependent on the distance between dots, a lower distance results in higher rate and better electronical coupling [29] ,[30].

The ability to choose the target ligand to certain degree, the availability of established techniques in literature and their efficiency in performing the exchange were suggesting that these techniques could also be applied to fullfill the goals of this work. In fact, supercrystals synthesized in this work can be regarded as nanoparticles connected along {100} facets and the oriented attachment process leaves {111} and {110} facets unchanged: because of this, the exchange mechanism explained earlier should be able to proceed in the same way as described for quantum dots.

The only concern that may be raised is due to the different geometries that characterize these structures, since the surface of an isolated quantum dots can be approached by any direction and thus ligands can freely diffuse and displace OA molecules, which is not true for more complicated structures, such as honeycombs. Unfortunately, it was not possible to find works in literature dealing with the post-synthesis passivation applied to supercrystals such as the ones used in this work.

Chapter 3

Experimental methods

3.1 Chemicals

Chemicals used in this work are listed in the table below.

Chemical	Abbreviation	Manufacturer	Purity
Ammonium chloride	NH_4Cl	Sigma Aldrich	$\geq$ 99.5%
Ammonium bromide	NH_4Br	Sigma Aldrich	$\geq$ 99.5%
Ammonium iodide	NH_4I	Sigma Aldrich	$\geq$ 99.5%
Hexadecyltrimethylammonium bromide	HTAB, CTAB	Sigma Aldrich	BioXtra $\geq$ 99%
Hexadecyltrimethylammonium chloride	HTAC	Sigma Aldrich	$\geq$ 98%
Tetrabutylammonium iodide	TBAI	Sigma Aldrich	98%
Methanol	MeOH	Sigma Aldrich	anhydrous $\geq$ 99.8%
Ethylene glycol	EG	Sigma Aldrich	anhydrous $\geq$ 99.8%
Acetonitrile	ACn	Sigma Aldrich	anhydrous 99.8%
Oleic acid	OA	Sigma Aldrich	anhydrous 99.8%
Hexane		Sigma Aldrich	anhydrous 95%
Toluene		Sigma Aldrich	anhydrous 95%
N-methylformamide	NMF	Sigma Aldrich	99%
N,N-dimethylformamide	DMF	Sigma Aldrich	anhydrous $\geq$ 99.8%
Ammonium sulfide		Sigma Aldrich	aqueous solution, 20%

All chemicalse were purchased and used without any additional purification steps. Simple ammonium salts (NH_4Cl, NH_4Br, NH_4I), HTAC, CTAB and TBAI were kept stored in a N_2-flow oven at 120 °C before use.

3.2 Synthesis methods

3.2.1 PbSe Quantum dots

All steps were carried out under N2 atmosphere with O2 and water levels below 5 ppm. Synthesis of PbSe NCs was performed using the procedure by Steckel et al.[steckel_1.3m_2003]. PbSe nanocrystals were synthesized as follow: lead oleate was synthesized first by mixing lead(II) acetate trihydrate (4.77 g), oleic acid (10.35 g) and octadecene (39.75 g) in a three

necked 250 ml flask inside a N_2-purged glovebox, heated up to 120 °C and left under constant stirring for 3 hour in order to properly degass the solution. Failing in doing so, will result in nanoparticles with a non-spherical shape [31] . In another flask 3.52 g of selenium, 0.41 mL of diphenylphospine (DPP) and 49.59 mL of tri-n-octylphosphine are mixed together and dissolved. The reaction proceed by heating up to 180 °C 20.5 mL of the previously synthesized lead oleate precursor and the quick injection of 15 mL of the selenide precursor. Growth proceed at 150 °C and it is quenched with the injection of 20 mL of butanol. The solution is allowed to cool down. Nanoparticles are precipitated with the addition of 10 mL of methanol, centrifugated at 2500 rpm for 10 min, the supernatant discarded and redispersed in toluene or hexane. These steps were repeated two more times. The final stock solution was stored in a N_2-filled glovebox

3.2.2 PbSe Supercrystals

All steps were carried out in a N_2-purged glovebox. Synthesis was carried out using a slightly modified version of the procedure described by Boneschanscher et al. [32] . Typical synthesis goes as follows: a small petri dish (diameter 3 cm) was filled with 5 mL of ethylene glycol. 4 μL of stock quantum dot solution with a concentration of 10^{-5} mol L^{-1} was diluted in 800 μL of toluene. 350 μL of this solution was dropcasted on top of the ethylene glycol substrate. After one hour, a brown film is formed at the liquid-gas interface and it can be scooped off using a suitable substrate and put under vacuum overnight to evaporate residual ethylene glycol.

3.3 Ligand exchange for supercrystals

3.3.1 Ligand exchange solutions

Solution of different molarities were prepared by dissolving a known amount of salt in a solvent. The various solutions are listed below. Sonication was used when needed in order to speed up the dissolution process.

Table 3.1: ***Ligands solutions****: solution prepared once and used for the whole work. A 20 mL vial was prepared for each solution. All solutions were stored in a N_2-purged glovebox.*

Ligand	**Solvent**	**Molarity** [mol L^{-1}]
Ammonium chloride	Methanol	0.08
Ammonium bromide	Methanol	0.08
Ammonium iodide	Methanol	0.08
HTAC	Methanol	0.18
CTAB	Methanol	0.15
TBAI	Methanol	0.10
Ammonium chloride	Ethylene glycol	0.08
Ammonium bromide	Ethylene glycol	0.08
Ammonium iodide	Ethylene glycol	0.08
HTAC	Ethylene glycol	0.18
CTAB	Ethylene glycol	0.15
TBAI	Ethylene glycol	0.10

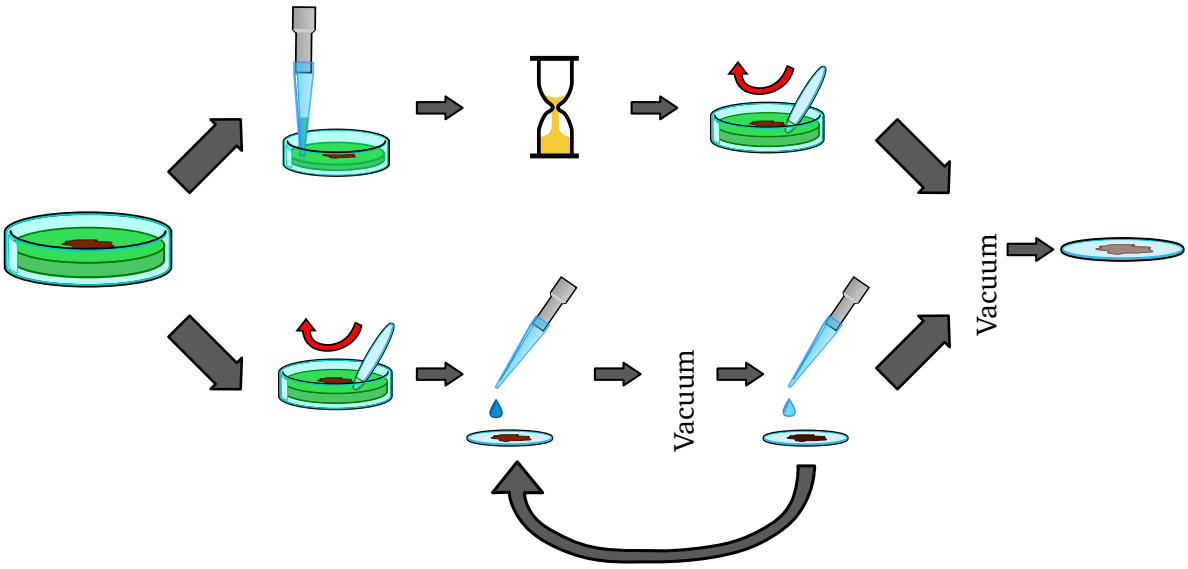

Figure 3.1: *Ligand exchange methods for supercrystals:* ***(top row)*** *in-situ ligand exchange. Starting from the assembled supercrystal, after the removal of a fixed amount of ethylene glycol (not depicted in the image), the ligand solution is injected directly in the ethylene glycol phase. Depending from the solvent used to dissolve the ligands, some time is waited, usually* 60 min. *After this, the monolayer is scooped from the interface as usual. Finally, the sample is placed under vacuum to remove possible organic contaminants.* ***(bottom row)*** *drop-casting ligand exchange. As soon as the superlattice is assembled, it is transferred to another substrate. The ligand solution is then dropcasted directly on the substrate, followed by a rinse with methanol and a brief exposure to vacuum in order to evaporate the organic solvent. These steps are repeated one more time, followed by a longer exposure to vacuum.*

3.3.2 Dropcasting method

All the following steps were carried out under inert atmosphere. Ligand exchange was performed using a modified technique described by Tang et al. [33] Ligand exchange proceeds as follows: after superstructure synthesis, the monolayer is transferred on a suitable substrate, for example a polymer coated copper TEM grid. After choosing a ligand from the table Table 3.1, 50 μL of this solution is dropcasted on it, rinsed with methanol and put under vacuum for 5 min to remove the excess organic solvent. These steps are repeated typically one more time. Finally, the system is rinsed by dropcasting methanol on the substrate and put under vacuum for 15 min.

3.3.3 In-situ method

All the following steps were carried out under inert atmosphere. In-situ ligand exchange was performed using a modified methdology described by Dong et al. [34] After superlattice synthesis, 150 μL of ethylene glycol was removed from the petri using either a 1 mL syringe or a standard finn-pipette. The same amount of volume was replaced with the ligand exchange solution. The system was left undisturbed for a variable amount of time, depending from the solvent used in the ligand solution. For example, based on the observations done in this work, samples exposed to methanol-based with solutions listed in Table 3.1 were left on the liquid phase for 30 min, while samples in ethylene glycol-based solution for 60 min.

3.4 Sample preparation

3.4.1 Standard scooping on TEM grids

Structures are synthesized using methods explained in this chapter. The resulting brownish film formed at the liquid-gas interface can be scooped using a copper grid coated with Formvar polymer and an amorphous carbon layer. The grid is left under vacuum overnight to remove excess solvent.

3.4.2 Standard scooping on other substrates

Samples scooped on other substrates (KBr, Gold, Amorphous silicon, Highly ordered pyrolitic graphite (HOPG), CaF_2) were prepared in the same way as TEM grids were made.

3.4.3 Superstructure detaching

Superstructures are absorbed at the liquid-gas interface, which may poses some problems for substrates sensible to polar solvents, such as KBr windows or hand-pressed KBr pellets.

It was noted that acetonitrile could be used to lift the superstructures from the ethylene glycol substrate. Since ethylene glycol and acetonitrile can form an homogeneous solution, care must be taken in order to perform this operation.

After synthesizing superstructures as explained in this chapter, acetonitrile can be poured very slowly with a finn-pipette or a syringe on the other rim of the small petri dish. Acetonitrile will not readily mix and due to density difference, it will form something similar to a two phase system, altough without a clear interface between the two phases. At this stage, superstructures will start to float on top of the acetonitrile phase.

Once the separation is achieved, it is possible to use the standard scooping methods used for the preparation of other samples, with the difference that the organic solvent will evaporate very quickly thus attaching the film to the substrate almost instantaneously.

3.5 Ligand exchange for other systems

3.5.1 Quantum dots

All the following steps were carried out under inert atmosphere. The methdology used here is one widely used in literature [25,36–38]. NCs were dissolved in hexane, while halide ligands were dissolved in NMF in an amount that varies with quantum dot's size, concentration and type of organic capping. In a typical ligand exchange with NH_4I, 1 mL of NCs in hexane were mixed with 1 mL of NMF containing excess NH_4I (20-30 mg). Upon vigorous stirring, quantum dots gradually transferred from the hexane to polar phase resulting in a colorless top phase in about one hour. The top phase was transferred in a new vial, rinsed with hexane to remove leftovers from the reaction and washed two times using toluene as anti-solvent and NMF as polar solvent.

3.5.2 Nanoplatelets

All the following steps were carried out in a N_2-filled glovebox. In a 6 mL vial, 2 μL of an 40% acqueous solution of $(NH_4)_2S$, 1 mL of NMF, 1 mL of hexane and 200 μL of nanoplatelets were

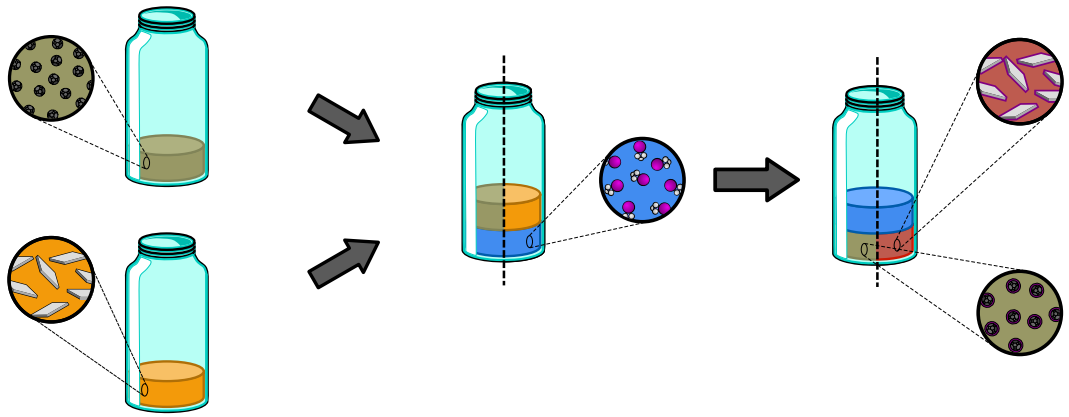

Figure 3.2: ***Colloidal atomic layer deposition (cALD)****: described in the work of Itthuria et al.* [35] *, this technique can be employed for nanoplatelets and quantum dots. From left to right: top vial contains quantum dots, while the bottom one nanoplatelets. From these vials, a new one is prepared with ligands dissolved in DMF. The middle vial is cut in half, meaning that conceptually the technique is the same for both systems. Another ligand is used for the platelets, but it is not showed in the image for clarity. After stirring, the system undergoes a phase swap and the nanocrystals suspended in the upper apolar phase migrate in the polar one at the bottom. A visible change in color was also observed for the nanoplatelets: from orange to deep red at the end of the process.*

mixed. The vial was stirred until complete phase transfer. The top phase was transferred in a new vial, rinsed with hexane to remove leftovers from the reaction and washed two times using toluene as anti-solvent and NMF as polar solvent.

3.6 Characterization

3.6.1 FTIR measurements

IR spectra from samples were collected using a Bruker Vertex 70 machine. Two different infrared windows were sampled: NIR (4000-10 000 cm^{-1}) and MIR (800-4000 cm^{-1}), using two different beamsplitters. By using the KBr beamsplitter, the whole spectral region could be sampled but, due to the features of the window itself, the signal-to-noise ratio in the NIR region was too high. In order to fix this issue, two different beamsplitters were used for the two different regions.

Region	Beamsplitter
800-4000 cm^{-1}	KBr
4000-10 000 cm^{-1}	Quartz

Spectra was averaged 64 times and resolution was set to 4 cm^{-1}.

3.6.2 TEM measurements

Transmission Electron Microscopy was done on a Technai 10 and 12 (FEI) electron microscope. The samples were collected on a copper grid coated with Formvar polymer and an amorphous carbon layer before the TEM measurements.

Chapter 4

Results and discussion

4.1 Synthesis of PbSe quantum dots

PbSe QDs were synthesized as described in the previous section. A TEM sample was prepared by dropcasting $20\,\mu$L of concentrated stock solution on a standard TEM grid. $20\,\mu$L of concentrated quantum dots solution were placed in a cuvette and solvent was evaporated by exposing the cuvette to mild vacuum for 1 min. 3 mL of TCE was added afterward in order to redissolve the quantum dots. The collected spectrum is shown in figure. Absorption peak and synthesized QDs spectra are showed in Figure 4.1

From the peak position of the first excitonic transition, the averate quantum dot diameter can be calculated [39] . The average quantum dot size was also calculated from TEM images by using a custom made Python program, briefly described in Appendix A. The program sampled about 150 quantum dots and from the length scale assigned to the single pixel the average diameter was be extracted. The calculated size was 6.06 nm, in agreement with the diameter obtained from the bare absorption peak.

4.2 Synthesis of supercrystals

Starting from PbSe quantum dots, superlattices were prepared as described earlier in the text. After synthesis, TEM samples were collected by scooping out the monolayer on the interface using a standard carbon coated copper grid. A typical sample is shown in Figure 4.2.

The experiment is influenced by many external variables and some of them are difficult to tune and control. Residues from the synthesis of the quantum dots may have an impact on the synthesis, since different concentrations of oleic acid on the surface can promote different types of superstructures [2,40] .

Under TEM, samples show a rich morphology composed of islands of one type of superstructure surrounded by other types of supercrystals and/or randomly attached quantum dots. There is no specific length scale for the diameter of these islands, but experiments shows a huge variation of this typical diameter.

By using 5.6 nm quantum dots, three facets are available for self-assembly. These facets, listed from the least to the most energetic ones, are: {100}, {110}, {111}. Among these three possibilities, only the first one is used by the oriented attachment process with this specific class of quantum dots. Most likely, this preference can be explained with the low the energy

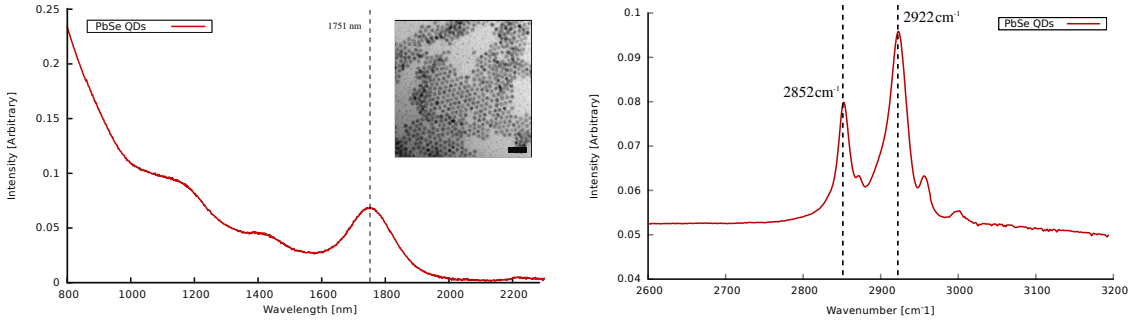

Figure 4.1: ***PbSe Quantum dots*** *- **a**: Inset shows a TEM image of the synthetized particles, with bar set at* 20 nm. *Infrared absorption spectra obtained for QDs used in this work is shown in picture. The dotted line is a guide for the eye that shows the position of the absorption peak, detected at* 1751 nm ***b**: Infrared spectra obtained for NCs, where oleic acid vibrational modes are visible. Two prominent peaks were detected, categorized as CH vibrations.*

associated to the desorption of oleic acid from the surface [41] and other dynamical equilibria between the gas-liquid interface and crystal's surface [11] . During this work, three main types of oriented attachment were observed: linear, square-like and honeycomb-like.

4.2.1 Linear attachment

Linear attachment can be seen in Figure 4.2. In this morphology, chains of quantum dots are atomically fused one to another in a linear fashion. Typical chains can go from three dots to tens of them, without any particular preference in size.

However, chains seem to prefer a direction for the attachment process. In order to understand this, it is useful to start with the simplest chain, the one composed of two dots. It is reasonable to assume that this structure will be adsorbed on the interface in a way that <100> directions will be either parallel or perpendicular to the interface. From this condition, the terminal dot will have only three out of six (100) available facets, since one is used to make the attachment with the rest of the chain and two are not accessible, because they are out of plane realtive to the gas-liquid interface and thus not available for further growth.

From these conditions, a dot can attach to any of these three available {100} facets on the terminal dot. A scheme where QDs lower their energy by fusing along the facet with the lowest surface energy does not work, since three different possiblities are available but branching is

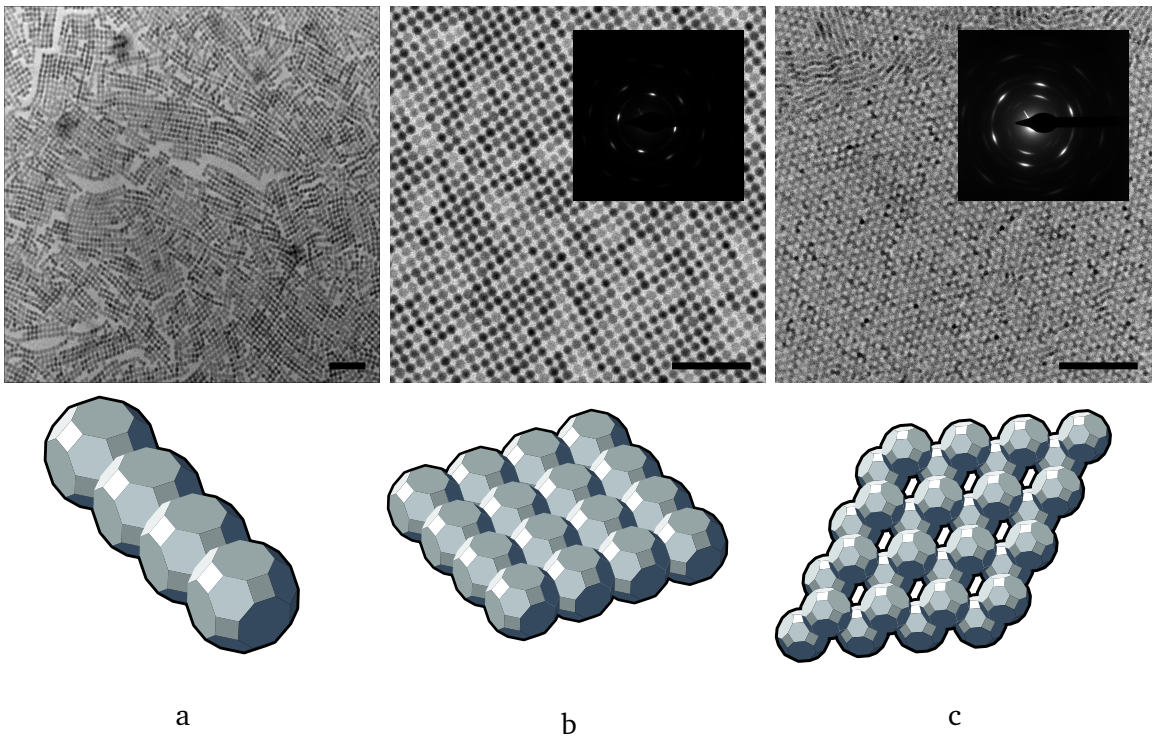

Figure 4.2: ***Observed attachment morphologies*** *- from left to right:* ***a.*** *example of linear attached quantum dots* ***b.*** *large area of square-like attached morphologies* ***c.*** *large area of honeycomb-like lattice. Insets in the middle and right images show the electron diffraction of the sample in the image. Bar is set at* 40 nm

not commonly experimentally observed [42] . This indicated that other factors have to play a role.

A possible explanation is due to dipolar interaction: Kortschot et al. [42] analyzed the equilibrium structures formed by PbSe and CdSe quantum dots and they have found out that quantum dots in solution tend to form linear structures in the same fashion as the ones observed in these experiments. The preferred orientation was explained in terms of minimization of dipole-dipole interaction energies, which are caused by the combined effect of higher order PbSe dipole moments, such as quadrupoles and octupoles: in particular, simulations showed that the unscreened octupole-octupole interaction is $-487\,\mathrm{kT}$ at $10.1\,\mathrm{nm}$ distance, hinting toward a possible source of long range interactions. However, as acknowledged by the same authors of the paper, the same nature of PbSe quantum dot permanent dipole is still an ongoing debate, since its direct measurements has not been reported yet.

Other papers also used this dipole interaction to explain the geometry of oriented attachment: in another work done by Cho et al. [8] , the synthesis of PbSe nanowires was explained through a dipole-dipole mediated oriented attachment along the (111) facet, altough in the paper also fusion along the {110} facets was observed.

4.2.2 Square lattices

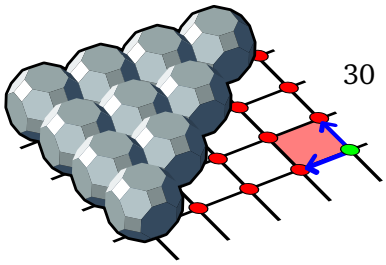

Figure 4.3: ***Square lattice****: the square structure is shown. Red dots represent projections from the center of each nanocrystals, forming a long ranged square grid. The red area represent a possible unit cell: experiments show that the angle formed by the two unit vectors is not exactly* 90° *but slightly less.*

Linear chains are an example of oriented attachment, they have long range order and thus they can be classified as one-dimensional crystals. The simplest two-dimensional supercrystal that satisfy the requirements of long range ordering and crystallinity are the square lattice. Shown in Figure 4.3, these structures were also the most common supercrystal observed during this work.

In the same fashion to what was observed with the linear chain, single dots are fused together along the (100) facet: but in this case *all* four facets perpendicular to the liquid-gas interface are fused with other dots, resulting in a structure that looks like a ordered sheet of connected quantum dots. In this case, dimensions can vary dramatically: from very small clusters (4 dots) to large ones, formed by thousand of nanocrystals and thus resulting in a structure that can be measured in squared microns.

In this case, little is known about the way this lattice is formed. By ignoring the issue posed by the lack of experimental evidence of PbSe dipole moment, one way to form these structure could be done by using intermediate steps formed by linear chains of varying or fixed sizes. But in this scenario, difficulties arise as soon as these intermediate structures start to interact, because dipoles are already lined up before reaching the final configuration. In the work of Talapin et al [13] , a possible scheme is presented: by allowing quantum dots to form a close packed configuration, the final structure is obtained by the alignment of quantum dots that minimize their dipole-dipole interaction energies.

4.2.3 Honeycomb lattices

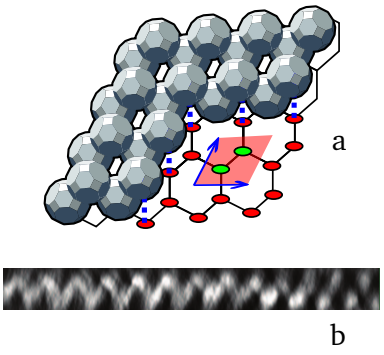

Figure 4.4: ***Honeycomb*** *- **a**: the underlying honeycomb grid formed by the honeycomb is shown. Red dots represent the projections of the nanocrystals on the plane, while the blue dotted line is used to highlight the out-of-plane configuration.* ***b****: the experimental out-of-plane configuration detected experimentally. Reprinted from Boneschanscher et al.* [32]

Another superstructure observed on the samples is the honeycomb lattice, visible in Figure 4.4. This graphene-like superstructures has interesting electronic features, which motivates the amount of work done in order to understand this particular structure. In fact, the determination of the actual morphology explained in two works [11] ,[32] presented significant challenges. Oriented attachment along any of the three possible facets allowed the self-assembly of graphene-like structures and so different geometries were proposed. Attachment through {111} or {100} forces a out-of-plane deformation in the structure, while no such deformation was predicted when using {110} facets. Because of the simplicity of the argument, this last geometry {110} was proposed as the most likely one, altough some issues were left unresolved at the time. By using a combination of HAADF, electron tomography and image recognition techniques Boneschanscher et al. [32] demonstrated that the actual attachment happens through the {100} facets. Even though the morphology of this supercrystal is known, the mechanism of formation of this superlattice is still poorly understood.

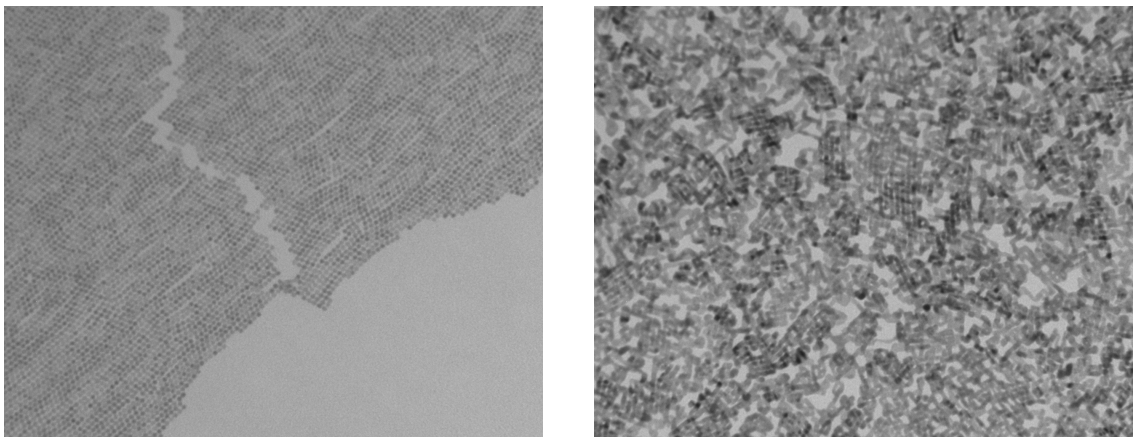

a. **b.**

Figure 4.5: ***Different growth medium*** *- **a**: Supercrystals grown on a liquid phase composed of 1:1 EG:DMF. The new substrate was able to substain oriented attachment. Structures synthesized on this substrate were mostly chains **b**: Sintered structures grown on liquid phase composed of pure DMF.*

4.3 Improving reproducibility

Experiments were performed under the same experimental conditions, altough some parameters could not be easily controlled: experimental parameters such as oxygen and water concentration were managed autonomously by the glovebox.

These factors, among others, are known to influence the outcome of the synthesis, as highlighted by the variety of different results imaged under TEM and obtained under comparable experimental conditions. This lack of uniformity on the surface is a known issue which is being addressed still today. Experiments performed in the past tried to highlight the effects that seemed to affect the synthesis the most. Factors such as temperature, solvent type and concentration were already explored by others [2,40] and same parameters were not explored in this work.

Surfactants were also explored as a possible driving factor for the controlled synthesis of honeycombs. Past experiments analyzed the impact of oleic acid [2,11] on the reaction. A broad range of concentrations were tried, ranging from 10^{-2}-10^{-8} $\mathrm{mol\,L^{-1}}$. But the only consistent result showed in both works is the the stopping of the attachment process due to the high amount of ligands at high OA concentrations. Other results showed in their works were not entirely reproducible.

These changes to the base protocol were not able to produce any quantifiable improvements in the likelihood to obtain honeycombs during synthesis, thus the base protocol without the annealing step was kept for the rest of this work. All synthesis were performed at room temperature and deviations from this protocol will be explicitly stated.

In this work, two other parameters were changed in order to see the effects on the outcome: evaporation rate and the type of substrate used during synthesis.

4.3.1 Evaporation rate

Evaporation dynamics in these system is particularly complex. Surface tension plays a prominent role. Surfactants can indeed lower the surface tension and promote the absorption of

nanoparticles on the surface. Some theoretical works agree with these results, as they predict a power law in respect to the growth of the islands and they make specific prediction about the nucleation.

Some experiments were carried out by placing samples under beker of different sizes. Three different bekers were employed: 250 mL, 500 mL and 1000 mL. Observed effects on the synthesis were not consistent or not useful in order to improve the quality of the synthesis. The smaller beker showed lack of attachment, while the other two containers showed either molten structures or normal attachment. When more than one sample was placed under the same beker, no attachment was observed in any of the sample.

How particles are scattered on the surface

4.3.2 Substrate

It is hypotesized that the substrate is responsible for the gradual destabilization of nanoparticle's organic capping by the solvation of oleic acid from the surface of the quantum dots.

Baumgardner et al. [43] investigated the formation of close packed configuration and the oriented attachment of quantum dots. Their experiments have shown that one factor needed to promote oriented attachment is the substrate's solubility of oleic acid. They have observed how compounds like acetonitrile, in which oleic acid is not soluble, oriented attachment was not observed while other substances like DMF readily showed oriented attached quantum dots.

These experiments explored only systems composed of quantum dots dropcasted on substrates and the insights gained were never applied to the synthesis of superlattices. In order to see if it was possible to replicate some of their results with our system, the same protocol used for the synthesis of our supercrystals was employed with only one change: the chemical compound used instead of ethylene glycol as a liquid substrate.

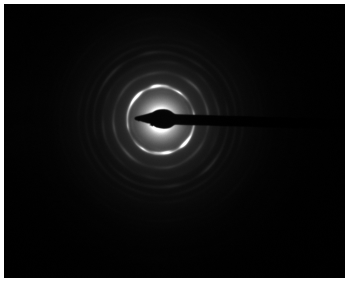

Figure 4.6: ***Orientational disorder****: ED pattern obtained from the sample shown in Figure 4.5. The lack of the typical fours peaks expected from square lattices can be interpreted as a lack of long range order.*

Two compounds were chosen from the list of chemicals tested in their work. Since no additional data was available to discriminate among those, DMF and methylformamide (NMF) were chosen based on the availability in the lab. Superlattice synthesis are very sensitive to any changes in the protocol. Because of this, DMF and NMF were tried in two different concentration: pure phase and a 1:1 mixture with ethylene glycol, in order to try the growth on a more diluted phase.

In the case of NMF no useful data was gathered because it was not possible to obtain TEM samples: in the case of the pure phase, right after the dropcasting of the diluted quantum dot solution on top of the substrate, the substrates started to boiling vigorously due to an unknown chemical intereaction and caused the organic solvent to evaporate almost istantenously obliterating any chance of film formation. The NMF/EG mixture 1:1 was less reactive but, again, the organic solvent was evaporated very quickly and a blackish film was formed in about 2 min on the surface. It was not possible to obtain useful information from the TEM sample, since the organic coating of the copper grid was completely destroyed.

When DMF was used as substrate, different results were obtained. In the case of 1:1 EG/DMF solution, quantum dots were arranged in a morphology similar to a square lattice.

Results are shown in Figure 4.5. However, even if the sample looked like a proper square lattice, the ED pattern collected for a large patch of structures showed a significant orientational level of disorder, visible in Figure 4.6.

Another interesting observation made during these experiments is connected to the speed of the synthesis. When using pure EG as substrate, monolayer is formed after around 20-30 min from the beginning of the reaction. By using these mixtures however the film formation was observed only after 5-10 min. Since the effects caused by different substrates to the synthesis process were not known, the brownish film was scooped out after 30 min instead of the more canonical 60 min used when growing structures on EG.

Effects from longer exposure to DMF are not known too, altough they may be inferred from the results obtained when using a pure phase of DMF as the liquid substrate.

Again, the film was formed on the surface before than the usual amount of time: after about 5 min. Some important differences with the 1:1 mixture were recorded: the film had the tendency of rip itself apart in more than one segment. After half an hour of reaction, a sample was collected on a copper grid and TEM images were taken. From the images it is possible to see that in the pure case the liquid phase has to be more “aggressive” than ethylene glycol in regard to the solvation of oleic acid.

Altough not enough experiments or analysises were performed to say anything quantitative, it is interesting to see how it is possible to obtain OA by so few assumptions and so few tries.

In particular, by changing the amount of exposure time on the DMF or the DMF to EG ratio results may be improved and better film obtained. Altough the synthesis on EG is the best tested and reliable one to obtain these structures, it is useful to known that also other ways can be used to otain similar results because more control variables may (or may not) allow a deeper understanding of the entire process.

4.4 Infrared characterization

Because of the low cost and relatively quick process, samples were initially deposited on hand-pressed KBr pellet. However data gathered using transmission Fourier infrared spectroscopy showed a consistent, strong and broad peak centered at around $3300\,\mathrm{cm}^{-1}$. Convolution with some other unknown signal was also observed, which resulted in a non-sensical spectra after the subtraction of the background. This source of noise was later traced back to water absorbed in the pellet from the atmosphere. Before changing the methodology, other ways to substract the background signal were tried with no results.

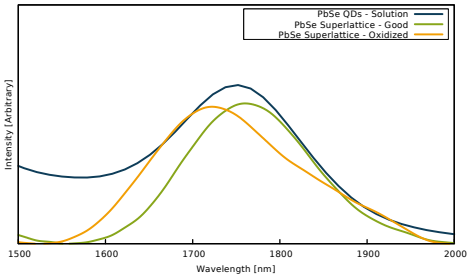

Figure 4.7: ***Oxidation****: Exciton peaks from two superstructures are compared to the absorption peak obtained for the same quantum dots in solution. When not properly handled, oxidation takes place quickly and it can be seen as a visible blueshift of the signal.*

To avoid the use of the hydraulic pressed pellets, a transparent KBr optical window was purchased. The organic coating that was protecting the hygroscopic material beneath it did not last more than two experiments before showing sign of degradation and occlusion. Due of this, substrate was later discarded and never used in this work.

In order to obtain clean spectra, another material was selected and the substrate was changed again to thin quartz windows. Collected samples were kept inside a custom built cell designed to avoid any contact between atmosphere and sample. However this device seemed to interfer with the workings of the IR spectrometer, since it was not possible to extract any spectra from both the UV-VIS absorption spectrometer and the FTIR spectrometer.

The collected signal, in both cases, looked like a sinusoid: this and other observations related to the way the cell was built suggested that issues related to refraction index mismatching were to blame, but no definitive answer was obtain. The usage of the cell was also discarded.

Samples were then collected on CaF_2 optical windows and samples collected by detaching superstructures from EG's surface through acetonitrile, as explained in the methods section. All measuraments were performed under ambient conditions. This choice is not optimal due to the easily oxidizable PbSe quantum dot's surface. The expected effect can be quantified in a blueshift in the absorption spectra, due to the etching of the surface of the quantum dots, which can cause significant blueshift in the absorption peak within two hours of air exposure [44] . This issue was essentially ignored for passivated samples, as they are protected by the halogen layer and should not be affected by normal atmosphere for short period of time [26] .

A more delicate question is raised for the unpassivated superstructures: to test the effects of air exposure, a sample of quantum dots dropcasted on the CaF_2 and left exposed to atmosphere for $30\,\text{min}$ showed no significant blushift compared to the spectra taken from quantum dots in solution.

When not properly handled, superstructures samples showed a blueshift comparable to $100\,\text{cm}^{-1}$ was observed. By taking some extra precautions, the blueshift was not observed in subsequent untreated samples.

When properly handled, samples showed instead, a small redshift and a broadening of the exciton peak. While the broadening of the peak can be most likely explained in terms of coupling effects arising from the nonuniformity of the sample on the surface, the redshift can be explained through many effects: energy level splitting, surface scattering or induced dipole-dipole interaction.

To analyze the sample using FTIR, two frequency windows were examined: $800\text{-}4000\,\text{cm}^{-1}$ and $4000\text{-}10\,000\,\text{cm}^{-1}$. The first frequency range is related to vibrations inside organic molecules present on the substrate, while in the second range is used to detect the excitonic transitions in the PbSe nanocrystals. The collected spectra for a untreated sample can be seen in figure [].

In order to exclude the presence of residues of other organic contaminants on the sample,

Table 4.1: ***Contaminants vibrational peaks***

Compound	**Wavenumber** $[\text{cm}^{-1}]$	**Assigned to**
Ethylene glycol	$3150\text{-}3400\,\text{cm}^{-1}$	OH vibrations
	$2935\,\text{cm}^{-1}$	CH_2 stretching
Acetonitrile	$2954\,\text{cm}^{-1}$	CH_3 stretching, medium
	$2266.5\,\text{cm}^{-1}$	CN stretching, medium
Methanol	$3328\,\text{cm}^{-1}$	OH stretching, very broad
Water	$3400\,\text{cm}^{-1}$	OH stretching, broad
N-Methylformamide	$3493.5\,\text{cm}^{-1}$	NH vibrations

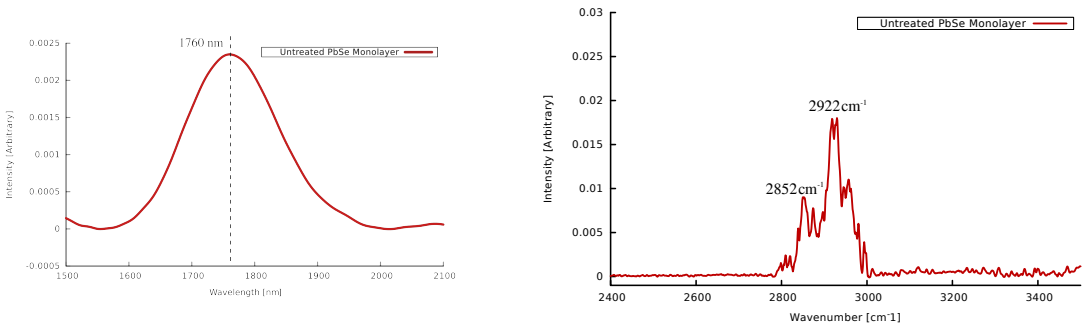

a **b**

Figure 4.8: ***Infrared spectrum of an untreated PbSe monolayer*** *- **a**: Absorption spectra, where the dotted line shows the position of the peak. **b**: oleic acid spectrum and vibrational modes*

peaks that characterize individual contaminant were collected and shown in Table 4.1. By checking the absence of any of these peaks in the sample, the presence of unwanted chemical species was ruled out.

The collected spectra in the mid-infrared region from an untreated sample of PbSe superlattice is shown in Figure 4.8.

Similar effects were also described in other works [6,20], where closed packed configuration of quantum dots showed unchanged absorption spectra. Anderson delocalization was used to explain this lack of coupling effects, and simulation performed by Artemyev et al [21] backed up the original hypothesis.

4.5 Ligand exchange

To reach the goal of this work, ligands have to be removed from the surface of these supercrystals, since they are a major obstacle to this type of investigation.

Previous work on the matter was done by Jaco et al., who employed Meerwein salts [45] to remove the organic capping from the nanostructures [40] . However, structures were damaged after the exchange procedure and it was not possible to check if OA molecules were removed or not from the surface of the superstructures. Also, the use of this particular compound was discouraged because of its bulky cations, which would have partially reintroduced the issue of noise.

In order to avoid these problems, another related technique was used. The idea was to borrow the knowledge developed in ligand exchange techniques applied to quantum dots solar cells. In this regards, these methods are used as a way to enhance the efficiency and stability of the quantum dots in the solar cell. PbS quantums dots are commonly used because of their tunability [46] that allow to match the solar spectrum absorption. These techniques are able to make PbS and PbSe nanoparticles stable under ambient conditions, and to increase the overall electrical properties of the cell: ligands such as oleic acid can decrease the coupling between dots by sterically separating every dots, while shorter organic or inorganic molecules can reduce the nanocrystal-nanocrystal distance thus increasing the coupling and charge transport properties.

In this work we are interested in the possibility of exchanging bulky organic molecules absorbed on the surface of supercrystals with shorter ligands, thus enabling the study of these systems with an STM microscope.

Works in literature explored a whole class of inorganic ligands [25 ,37 ,47 ,48] used to solve the aforementioned issues. The paper from Zhang et al. [33] was chosen as a starting point, because of the efficiency reported in the paper in regard to oleic acid removal and the almost unchanged exciton peak found in the nanocrystals after treatment, essential properties needed

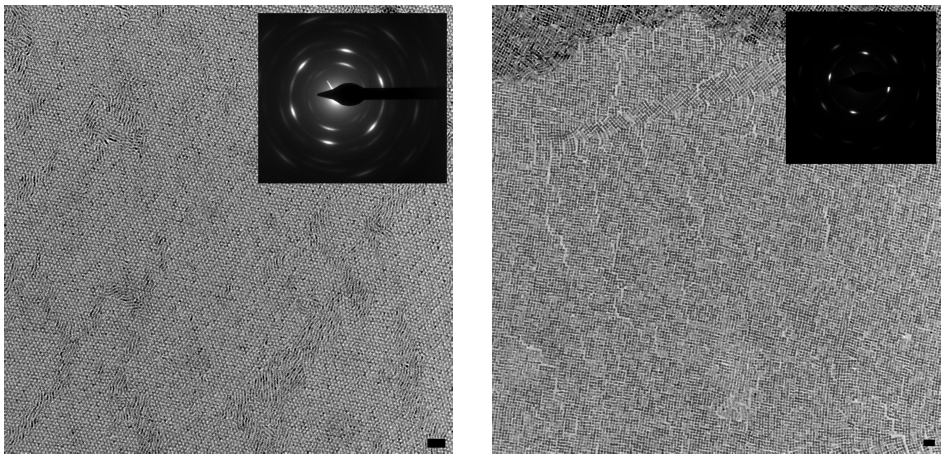

a **b**

Figure 4.9: ***TEM images of a sample after HTAC treatment*** *- **a**: honeycomb superstructures and **b**: square superstructures, in both cases there was no detectable damage imparted to the supercrystals . TEM sample was obtained with two repeated cycles of passivating solution and washed with methanol. Inset is electron diffraction pattern found for the sample in the image. Bar is* 20 nm

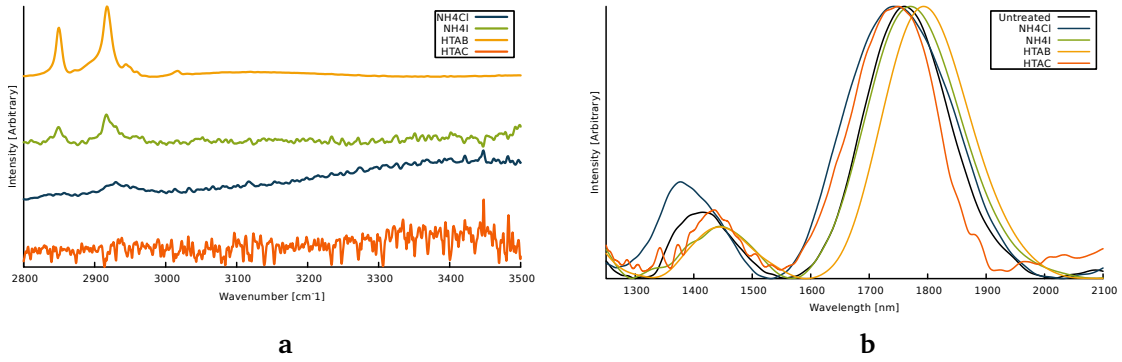

Figure 4.10: ***Ligand exchange on substrate*** *- **a**: Collected spectra for treated samples in the MIR region. Chlorine based ligands (HTAC and NH_4Cl) managed to remove OA from the sample as the related peaks are not visible in the spectra anymore. Iodine based (TBAI and NH_4I) compounds and HTAB did not succeeded in a complete removal, as significant signal related to oleic acid is still detected from the sample after treatment. In particular, ammonium bromide and TBAI are not shown in the figure, since no working sample was obtained with these ligands.* **b**: *Absorption peaks collected in the NIR region. The black line is the absorption peak from the untreated superstructure. NH_4I and HTAB display a measurable redshift, while HTAC and NH_4Cl are slightly blueshifted.*

for the task at hand. However this method was applied to PbS quantum dots and, altough very similar to PbSe ones, there was the chance that the two systems may have behaved in different ways.

This issue was addressed by complementing the techniques used in the aforementioned paper with other works from literature, that dealt specifically with the passivation of PbSe quantum dots. In particular, in the work of Woo et al. [26] , simple ammonium salts are described as an efficient and cost effective solution to ultrastable PbSe quantum dots. As explained in this paper, the first excitonic absorption peak did not change much after treatment in both position and FWHM: absorption peak was redshift of about 5 nm.

However, the methodology used to deliver the new ligands described in these experiements was not compatible with our system. In the works cited above, samples were prepared by spin coating a layer of quantum dots, passivation was performed by dropcasting the ligand exchange solution and these steps were repeated six or more times. Supercrystals instead are grown on top of a liquid substrate and spin coating is not an option due to how crystals are formed.

Different ligand exchange strategies were tried and two different protocols were developed, tested and characterized using infrared spectroscopy. Ligands tested included both simple ammonium salts (NH_4Cl, NH_4Br, NH_4I) and complex ionic surfactants (HTAC, CTAB, TBAI).

In order to screen for ligands that may destroy supercrystal upon passivation, these ligands were dropcasted directly on samples prepared on TEM grids as described in methods section. Using TEM, samples were imaged in order to understand which ligand was able to strip off the organic layer without damaging the superstructures. TEM images for this first screening are visible in Figure 4.9. For all ligands, it was found out that no significant changes were visible at this stage.

4.5.1 On substrate

There is a significant discrepancy from what was obtained during this works and the results published in the literature [33] . Some of these discrepancies can be explained in term of the different protocol used to prepare and collected the absorption spectra. In fact, the original protocol was changed in order to get it adapted to our system: differences can be summed up in the lack of multilayers and multiple washing steps.

In the original protocol, samples were prepared by spin-coating multiple layers of a diluted solution of quantum dots on a suitable substrate, followed by the application of the ligand exchange solution. By placing multiple layers on a single sample, signal was boosted significantly, thus making it clear and less susceptible to noise.

The same approach was tried also in this work, but placing a second layer on top of a previously deposited one resulted in the detachment of both as soon as the substrate was partially submerged with EG, as required by the scooping technique. For the rest of this work, a single monolayer was used per sample.

A possible explanation for this behavior may be connected with the different surface stabilisation found after passivation: superstructures are not sterically stabilized anymore, and the ion-cation on the surface form a charge double layer that electrically stabilize the structures. Because of this, passivated superstructures have an high affinity for any polar compound such as ethylene glycol. In fact during the deposition of the second layer, the first one was consistently detached from the solid CaF_2 substrate and started floating on the gas-liquid interface. Other film deposition techniques were not tried, as it was deemed more practical to deposit a single layer.

The number of washing steps made with methanol were also reduced based on these observations: being an highly polar organic solvent, effects observed for ethylene glycol were comparable to the ones observed during these washing step. After the first passivation step, supercrystals deposited on the surface were lifted from the substrate and started to float on the methanol-gas interface upon the addition of any methanol solution, with or without ligands dissolved in it. The high vapor pressure of this compound results in high evaporation rates, thus fast a fast interfacial contraction which resulted in mechanical stress that caused visible shrinking and tearing of the supercrystals.

Also the number of times that the ligand solution is dropcasted on the sample, altough not stated in the original paper [33] , was found out to be quite important. One single step was consistently incapable of removing most of the oleic acid from the sample, but applying more than two passivation steps increased significantly the chances of running into the same problem described earlier, since ligands were also dissolved in methanol.

The type of ligand used, in particular in relation with the halogen used for passivation, seems to play a role as well. The type of ligand seem to enhanced the destructive phenomenon observed. Chlorine based ligands such as HTAC or NH_4Cl seemed to be quite unreactive, while the opposite was found to be true for the iodine based counterparts where, most of the times, superstructures were litterally torn to pieces upon the addition of the methanol-ligand solution. Effects due to bromine were found to be in between these two extremes. This trend was not connected with the specific chemical structure of the ligand, since same behavior was found for both ammonium salts and the bulkier cations, hinting to the type of halide as a possible way to explain different reactivities. Without more quantitive data, it is not clear if this is only a coincidence or a valid observation.

These issues were partially addressed by reducing the number of washing steps to one

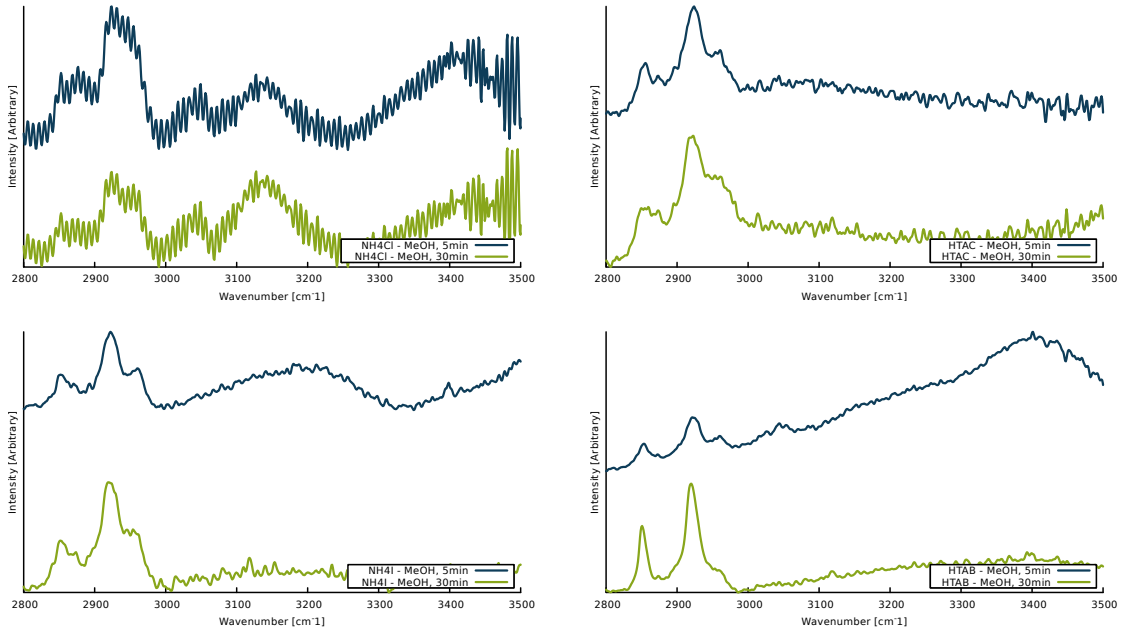

Figure 4.11: ***In-situ passivation with methanolic solutions****: NH_4Cl (**top row, left**) shows leftovers from the ligand exchange where, altough not perfectly clear, signals from the ammonium group can be seen. Due to the low quality of the spectra, it is not possible to say if oleic was removed after half an hour. HTAC (**top row, right**) showed an almost unchanged spectra and time seem to have not played any role. NH_4I (**bottom row, left**) also showed similar problems found with HTAC. (**bottom row, right**) HTAB showed the ability to remove organic ligands, altough not completely. Overally speaking, results are far from optimal for every single ligand.*

and to increase the number of passivating steps to two: in this way there is an higher chance of performing a complete exchange, altough traces of oleic acid may still be present on the surface.

4.5.2 In-situ

In order to solve all the issues given by the ligand exchange process performed directly on the CaF_2 substrate, another technique was developed and tried. Based on the experience gained while trying to dropcast method, it was assumed that damages imparted to the superstructures could be traced back to methanol: the polar solvent was able to solvate the entire structure, while its evaporation crumbled and shredded the structures previously located on the surface of the substrate. Since methanol was the solvent used to dissolve the ligand and also for the final washing step, in order to reduce these damages the new technique had to be effective not only in term of ligand removal but also it should have avoided the use of highly polar organic solvents such as methanol.

In literature, works dealing with the passivation of superstructures are essentially non-existent. The closest system found in literature that dealt with this topic was done by Dong et al. [49] , dealing with the in-situ ligand exchange on a superlattice made of gold nanoparticles grown on a liquid substrate. Ligands were injected directly in the liquid phase and the monolayer extracted as a normal film.

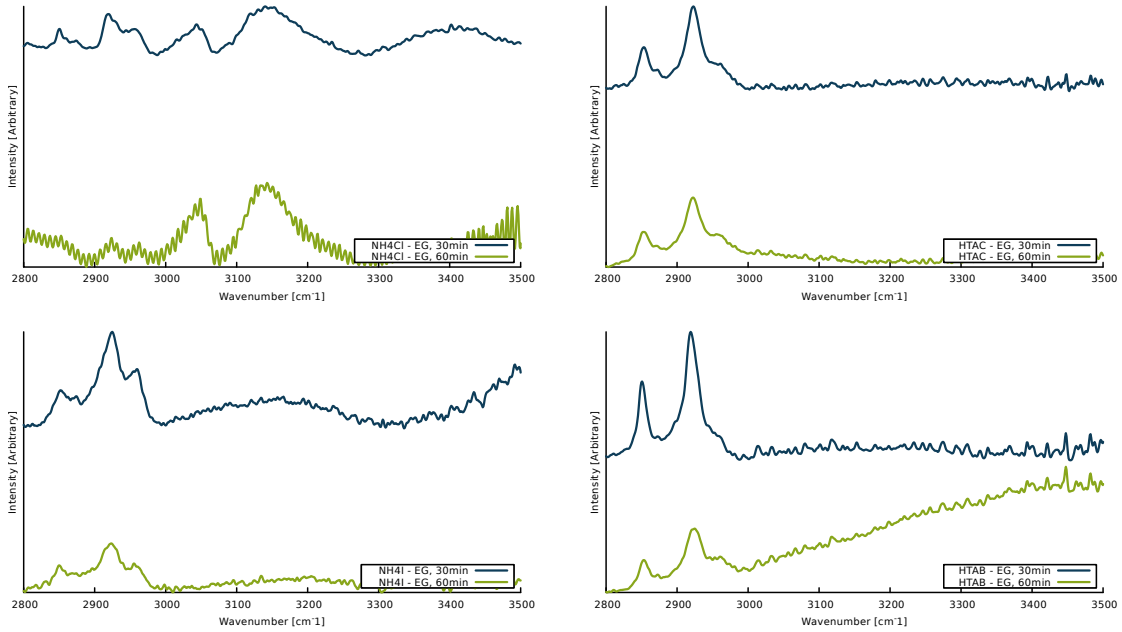

Figure 4.12: ***In-situ passivation with ethylene glycol solutions****: NH_4Cl (**top row, left**) shows leftovers from the ligand exchange where, altough not perfectly clear, signals from the ammonium group can be seen. Due to the low quality of the spectra, it is not possible to say if oleic was removed after one hour. HTAC (**top row, right**) showed to be able to remove the OA, altough residues are still present. NH_4I (**bottom row, left**) also showed the ability to remove the organic capping, altough residues are still present. (**bottom row, right**) HTAB showed the ability to remove organic ligands, altough not completely. Overally speaking, the situation found here is comparable with the one found when using ligands dissolved in methanol-based*

The methodology employed in this work was very similar, but with a different type of liquid phase and ligands were dissolved in other types of solvents. In order to avoid deviating too much from the working experimental procedure, ligands were dissolved in methanol. Injection was performed directly in the liquid phase, as in the previously cited work. The detaching procedure explained in the method section was used to lift the passivated structure from the surface. It was noted that this step not only served as a simple way to lift the structures from the gas-liquid interface, but also as a washing step, thus removing unbound oleic acid from the surface of the nanocrystals and other solvents residues, such as ethylene glycol.

Two different exposure time were chosen for this experiment: 5 min and 30 min. Altough ligands are dissolved in methanol, it is likely that a significant fraction of the ligands will have to diffuse inside the liquid phase. Since it is not possible to reasonably quantify this amount of time, in order to explore effects at short time scale and at the long one, the aforementioned times regimes were selected.

Results for this experiments are shown in Figure 4.11.

Results obtained through dropcasting and this technique showed similar behaviour. When ligands such as NH_4I or TBAI dissolved in methanol, a behaviour similar to the one described when using dropcasting technique was found, damaging the brownish film at the liquid-gas interface and thus ruining the sample. The problem was traced, most likely, back to methanol: at the moment of injection, the ligand solution migrates to the surface of the liquid substrate, inducing hydrodynamic currents and other disturbances that resulted in mechanical stress the

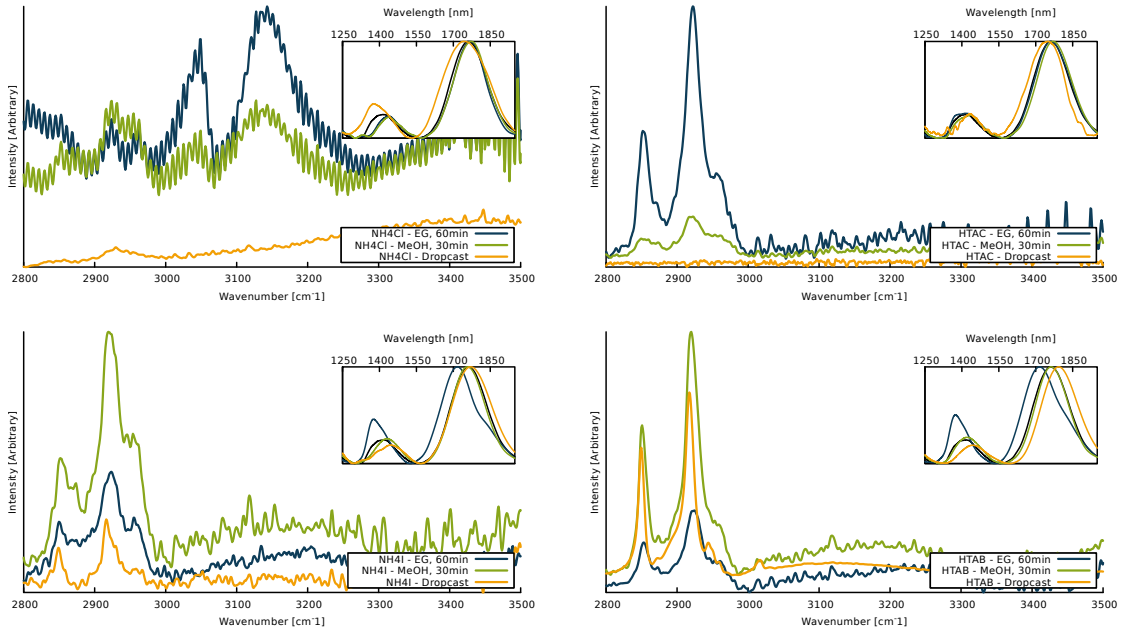

Figure 4.13: ***Final comparison*** *- Comparison between three methodologies employed in this work. Unsurprisingly, methanol-based solutions seems to behave better in all environments compared to the EG-based counterpart.*

monolayer and thus comparable effects observed during dropcasting.

In order to fix this issue, ligands were dissolved in ethylene glycol. Changing solvent however is a decision that must be taken carefully, since methanol takes active part in the ligand exchange process and two important factors can potentially vary: the time necessary to perform the exchange and the effectiveness of the exchange process [33] .

For the first parameter two different time regimes were selected: 30 min and 60 min. These time scales, longer when compared to the methanol case, were selected to reflect not only the unknown factors connected to the solubility of the byproducts of the ligand exchange, but also to the higher viscosity of the liquid substrate. Comparison between different running time are shown in Figure 4.12.

Results show how longer times were actually a better decision: the procedure, when stopped after 30 min was not able to remove OA in almost every case. However, after one hour, the procedure showed no traces of OA, sign that oleic acid was removed from the surface of the superstructures.

4.5.3 Two methods compared

An overview of the results obtained with two methods tried in this work can be seen in Figure 4.13. It is possible to see that OA signal can still be detected with both methods: this can be interpreted either as a sign that oleic acid molecules were still attached on the surface of the superstructure, or that the samples were not properly washed. In order to discriminate between these two options, a proper washing protocol should be developed. During this work, toluene was tested as a way to clean samples: due to its apolar nature, the monolayer remained attached to the substrate upon the dropcast of the solvent. However, this was tried only at the

end of this work and no conclusive data was gathered.

Ligands characterized by either iodine or bromine ions, regardless of the molecular structure of these ligands, failed to perform a complete exchange and/or mantaining the exciton peak unchanged. In both cases of bromine and iodine, organic signal could still be detected and in one case the exciton was visibly blushifted. HTAC and NH_4Cl were the most successfull ones: they were able to perform a complete exchange with at least one method, leaving the position of the exciton peak almost unchanged. These two ligands are the best candidate found in this work.

From a methodological point of view, the in-situ passivation has failed to obtain the desired results: in this context, the best results were obtained using ligands still dissolved in methanol, which partially destroy all the benefits in using this technique. Ligand exchange in ethylene glycol doesn't work as expected: a possible explanation for this can be traced back to the solubility in ethylene glycol of the intermediate byproducts of the procedure, as explained in the supporting material of the work from Tang et al. [33] . However, since there is no easy way to swap ethylene glycol for another liquid substrate, there are no added benefits for using this technique. The dropcast method was the only method who was able to perform a complete ligand exchange, and as such it is the only technique that at this point can be used to passivate superstructures.

Chapter 5

Conclusion

PbSe supercrystals were synthesized successfully using the experimental protocol used in this work. In particular, square and honeycomb lattices were obtained many times, where the former were found during experiment more ofter than the latter. This issue is connected to the low reproducibility rate of the experiment, which is a well known problem that is being addressed.

To address this problem, parameters such as evaporation rate, oleic acid in the substrate and others were suggested during this work as a possible way to address them. Experiments performed showed no statistical improvement on the protocol by changing any of the aforementioned parameters. However, the number of experiments performed on the matter is not enough to say anything final and future works in this direction may shed more light on the issue. For example, recents works [2] may suggest that a controlled evaporation promotes the growth of square lattices, which is in agreement with the most recents findings on similar systems.

Growing supercrystals on other substrates was demonstrated. Experiments performed showed the growth of oriented attached structures on a mixture of 1:1 EG / DMF. However, electron diffraction shows some degree of disorder on the NC scale and thus more research on the matter is deemed necessary.

Ligand exchange was performed using 2 different methodologies: by dropcasting on the as-formed superstructure, and in-situ while the superlattice is still on the ethylene glycol layer. The former showed an effective removal of the capping ligands, confirmed by the disappearance of the relevant vibrational peaks associated to oleic acid after treatment. However, some experimental issues connected were also observed: superstructures tend to be destroyed during the procedure due to factors that are not completely related to the ligand exchange procedure itself. Because of these observations, this technique was deemed not optimal in order to obtain samples for the STM. The in-situ technique solved some of these problems while introducing new ones. By keeping the supercrystals at the liquid-gas interface, the observed degree of degradation caused by the procedure was almost non-existent when methanol was used as solvent for the ligands, while essentially no damages or mechanical stresses were observed when ethylene glycol was used as a solvent. However, the insitu methodology is not as reliable as the dropcast one: results reported here shows that it is not always possible to achieve a complete removal of the organic capping from the superstructures.

It was not possible to obtain a working sample for the STM. It is not clear why: samples were prepared with both methologies without obtaining any useful results. In particular,

HOPG samples were consistently found devoid of any superstructures. Removing the ligand exchange step was not helpful either, since no improvements were obtained in that regard. Considering works previously done on the same type of system [40] , the lack of results may be due to mistakes made during the preparation of the HOPG samples. Some initial results were obtained using the ambient AFM, where a sample showed clusters of quantum dots with a geometry comparable to that of a square superlattice.

Chapter 6

Outlook

Results are difficult to understand for different reason, mainly because there is no easy way to understand if the signal assigned to oleic acid is gone or not. Future works in this regards should probably start by obtaining a calibration curve and cross check these results with another techniqe, such as nuclear magnetic resonance (NMR).

Ligand exchange on substrate may work with other solvents. In order to increase the reliability of the insitu technique, more parameters have to be varied. For example, molarity of the solutions used with this method was not changed during this work.

To make this technique "bullet proof", more checks are necessary. Altough works in literature often consider successfull the exchange by only using colloidal stability and the lack of oleic acid vibrational peaks in the IR spectra, systems explored in this work depends on more variables than the simple colloidal quantum dots from which they are composed of. In this case, it would be beneficial to probe directly the surface to check the actual distribution of halides on the surface of the superstructures.

The detaching of the superstructures from the liquid-gas interface could be employed in further investigation of the interaction between liquid substrate and supercrystals or to investigate the dynamics behind the self-assembly procedure. Preliminary results showed that it is possible to obtain square-like structure on a mixture of 1:1 Ethylene glycol / DMF, and there are no indications that this result cannot be further improved. In particular, it would interesting to inspect different combination of quantum dots and substrates, with other nanocrystals that are known to not behave well on ethylene glycol. CdSe nanoparticles are one clear example on this regard.

Reproducibility, along with the non-uniformity of the sample, are the two biggest practical issues. For the former, inspiration can be taken by other recents works in literature: for example, experiments have shown how oleic acid can impact the outcome of the synthesis even at low concentration and it is very likely that residues from the synthesis process are carried throught even the most careful sequence of post-synthesis washing steps. As a starting point, the complete removal of these residues would be something desirable, since it would allow a better understanding of the interaction between ligands and self-assembly. One way to achieve this would be increasing the number of washing steps, but the repeated use of non-solvent such as methanol, ethanol or buthanol results in gradual permanent destabilization of the organic capping and thus loss of colloidal stability. A solution to this problem is given by acetonitrile, because it can act as non-solvent but it doesnt destabilize the organic layer even after repeated applications, thus allowing an experimenter to greatly reduce the amount of residues from the

reaction.

After this, effects of oleic acid on the outcome of the synthesis could be performed using a Langmuir through. In particular, it would be interesting to see if the buckling could be explained in terms of some kind of critical behaviour around a precise and reproducible surface pressure. This setup would be also interesting to check the dependency on other effects, such as depletion interaction.

Non-uniformity can be caused by many external factors, but one possible way to reduce non-reproducible effects could be attained through the reduction of the surface available to evaporation: in our current protocol, the diameter of the petri dish used to contain the liquid phase. Changing the surface area however will force a complete revision of the protocol: for example, concentration will have to be changed forcing the execution of many different experiments. One way to speed up this search could be accomplished by borrowing techniques from combinatorial chemistry, where many reaction conditions are tried in parallel thus cutting down the time necessary to find the new working experimental conditions significantly.

Another hint on how to improve on reproducibility may comes from the inkjet printing industry. An inkjet printer has to be able to deposit an uniform layer of ink in a reproducible manner: from these prerequisites lots of simulations, theories and models were developed in order to understand how a solution of dispersed particles in the micro and nanoscale range can be deposited uniformly. In other words, the physics behind these processes is quite similar to the one found in at the early stages of the self-assembly process. Insight gained by this field may help to understand how the early stages of the self-assembly process may influence the final ones.

Appendix A

Features detection in Python

Abstract

TEM images are routinely used to extract information about a quantum dot population. In this report, a program that was developed to extract and calculate diameter, angles distances between quantum dots in a square lattice is presented. Advantages and disadvantages from previous methods are also reported and a brief explanation on how the program works and what all the parameters do is given.

Introduction

TEM (Transmission Electron Microscopy) is a widely used technique to image samples at the micro/nano scale. By shining a stream of electrons through a very thin sample, a black and white image can be reconstructed from the intensity of the transmitted electrons.

These images, when coupled with other information such as the resolution per pixel, can be used to extract lots of information about the sample itself. Quantum dot's size distribution is routinely extracted in this way and checked against other empirical methods used to calculate the average size distribution from the absorption peak. But the size distribution is not the only information stored in these images: since they are direct representation of the surface of the sample, every geometrical information is stored in these images.

In order to collect this data, two approaches are available: human or computer based. The first one involves one physical person to look at the images and manually extract all the interesting features. However, this task is particularly time consuming and prone to human error but it can ensure a good level of accuracy. This approach becomes quickly inefficient as the dataset grows.

On the other hand, a computer can extract the features that we need and the time required to perform this operation (even on large dataset) is dramatically reduced. However, in this approach we lose the reliability of the human operator and errors can be introduced systematically.

To overcome this problem, an approach that mixes these two point of views together was developed. The core idea is letting the program to swift through the dataset and to look for features that are described by parameters decided beforehand by an human operator. Then, the human operator can tweak these parameters in order to exclude different dots: in this

way, it is possible to retain a good compromise between the precision gained from an human operator and the speed that at which these object recognition tasks are done on a modern computer.

Works in this direction were already performed by Mark Boneschauser, who wrote a MATLAB script used to extract features such as dot-dot distance from TEM images. However the program was relying on lots of parameters and lots of tweaking was necessary in order to adapt the script to other images. In order to obtain high quality data, the script was supposed to be tweak manually for each image. In this report we present a new approach to the same problem using algorithms developed for image and pattern recognition, where the human intervention is still crucial but the amount of time and tweaking necessary in order to obtain results of comparable quality is drastically reduced. This is achieved through the combination of an user interface and a different approach applied to the image processing.

Methods

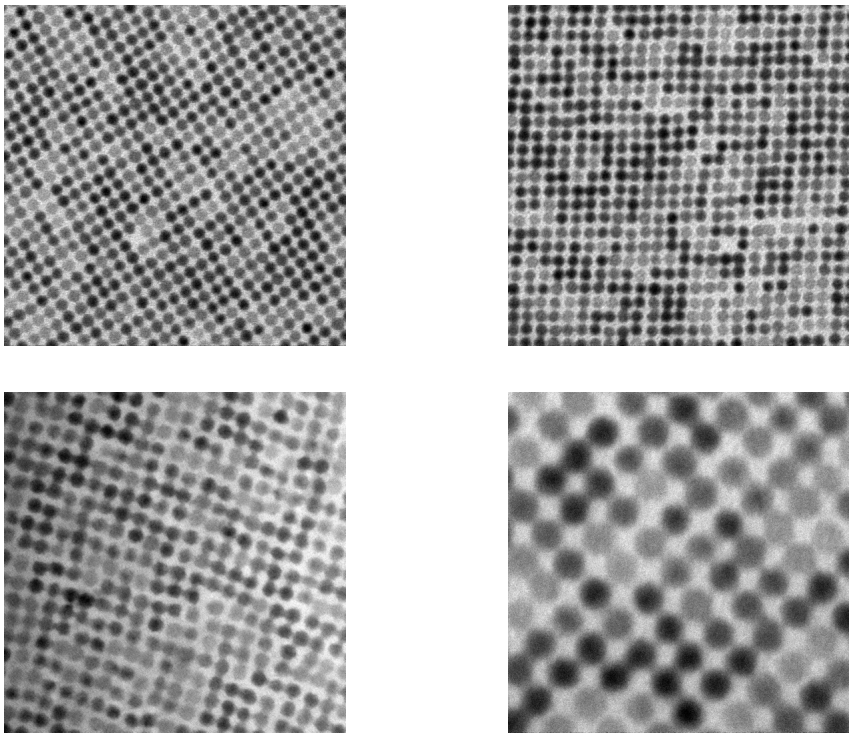

Figure A.1: *Example of oriented attachment*

In order to extract features in a reliable way, images are preprocessed first. This means that the background noise that is usually captured in a standard TEM image is filtered using two *denoising algorithms*. In this report, these algorithms are treated like blackboxes, since a deep explanation of how these algorithms works is out of the scope of this document. The purpose of these preprocessing steps is to render the image as homogenous as possible by averaging high frequency noise that is usually recorded in this type of images. Since we are not looking for a general purpose solution, these algorithms are able to reduce the noise while mantaining

an high contrast between foreground and background.

Next, the background is removed with an adaptive algorithm, which is able to distinguish between objects in the foreground and background automatically. However, the efficiency of the algorithm strictly depend on the level of constrast: if it is not high enough, this algorithm will fail to distinguish the two and the image will not be usable for the next steps.

Once the background is discarded, the output will be a black and white image containing the outline of the features (in this case, quantum dots) in the image. From the outline, it is possible to extract the centroid (i.e. the center of every single spheroidal object detected). From this bit of information radius, diameter, dot-dot distance and dot-dot angles can be computed in a fairly accurate way.

As stated before, the program is not a general solution for any type of images and as a such some assumptions about the input images were made. Only quantum dots are recognized at this stage, and other objects in the image will be treated in a equal way, leading to inconsistencies in determination of the average radius and reciprocal angles. Images must be taken in such a way to have a consistent background. Finally, the contrast must be high enough to allow the algorithm to understand what is the foreground and the background. Empirically, if the image has a uniform background and dots are clearly visible in the image, then the program will be able to discern between the twos without any problem.

Results

Some examples of the program ability to detect centroids are shown below. In the following table are reported the values need to reproduce the output.

	Sample Figure A.5	Sample Figure A.6	Sample Figure A.7
Method	Adaptive	Adaptive	Adaptive
Denoise Weight	0.001	2.0	1.0
Length Scale	100.0	60.0	50.0
Distance cutoff	0.5	0.55	0.45
Area cutoff	0.0	0.0	0.0
Minimal structure cutoff	90.0	35.0	25.0
Maximal structure cutoff	138.0	52.4	37.0

The obtained distances and angles for all samples are shown below. The graphs on the left is related on the distances between quantum dots: on the horizontal axis we have the distance expressed in pixels while on the vertical axis we can find the relative count. The graphs on the right is related to the angles between quantum dots in the image: the horizontal axis is the degree, while the vertical one is the count.

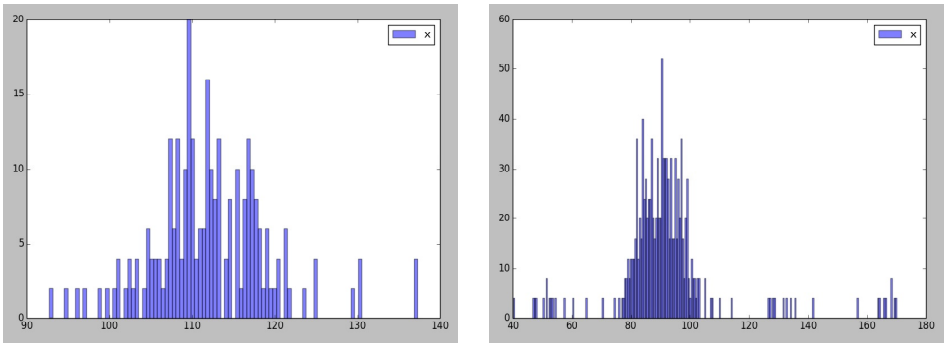

Figure A.2: *Distances and angles for sample Figure A.5*

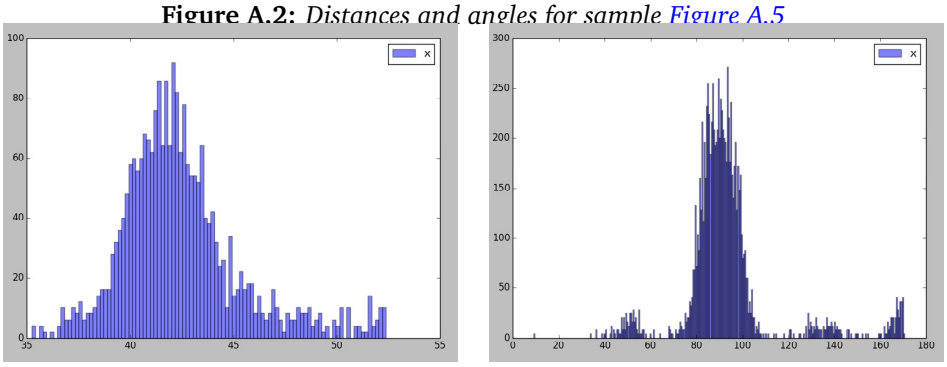

Figure A.3: *Distances and angles for sample Figure A.6*

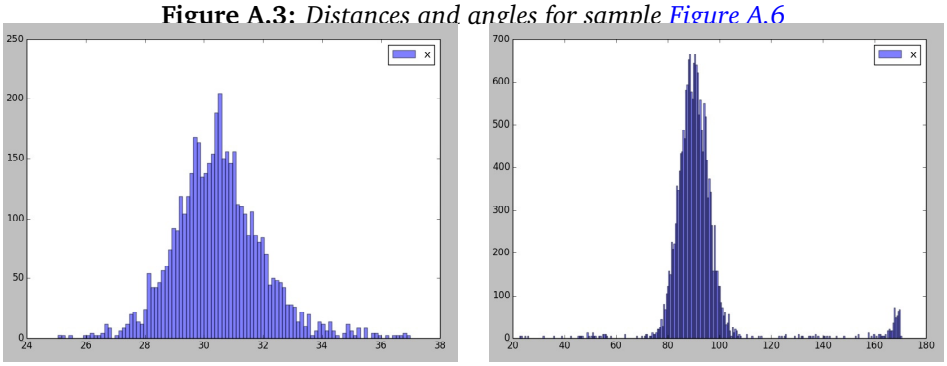

Figure A.4: *Distances and angles for sample Figure A.7*

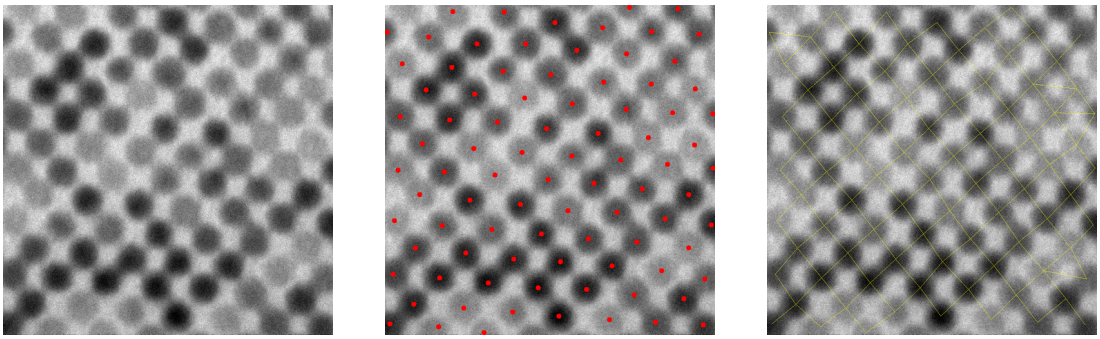

Figure A.5: *Sample Figure A.5. From left to right: input image, detected centroids, calculated neighbours*

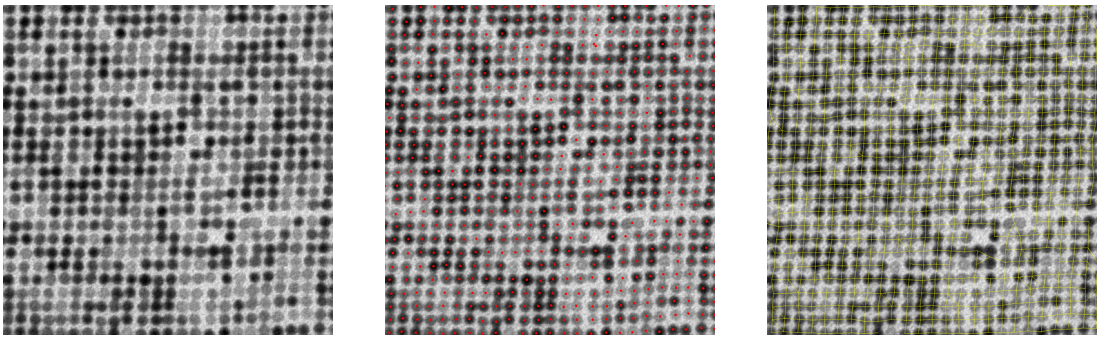

Figure A.6: *Sample Figure A.6 . From left to right: input image, detected centroids, calculated neighbours*

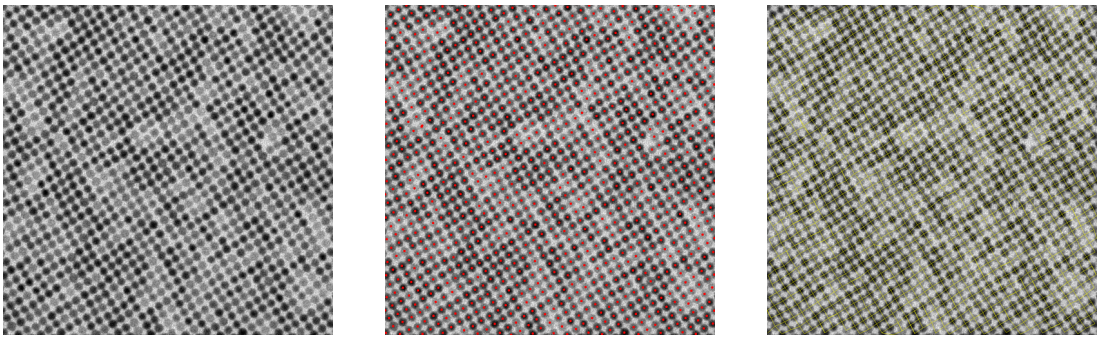

Figure A.7: *Sample Figure A.7 . From left to right: input image, detected centroids, calculated neighbours*

Discussion

The samples showed in the results section have an average quality. This means that increasing the quality (in this context this means high contrast between foreground and background and low noise) will improve the output of the program. But even with a medium to bad image quality, the program will be able to work fairly good.

The first and the last samples share a common structure, as it possible to see from the angle distribution. The sample in the middle show a strong peak around 90 degrees plus two small simmetric clustering at around 50 degrees and 130 degrees.

We must note hovewer that the shape of the distribution is not completely determined by the characteristic of our samples. This is due to the way we extract the centroids from the image: since they depend on the parameter that we are using to detect them, changing parameters will change the them and the angle distribution as well. On top of this, changing the position of the center of the particle by some pixels, will change the value of the estimated angle by some degrees and thus it is something that cannot be overlooked. The same argument hold for the distances distribution, even if the problem it is less important for this quantity, due to the fact that the associated error introduced by varying the distances by, for example ten pixels, on average will change the final distances by Angstroms or even less.

The distribution is also modified by the quality of the centroids detection and the extracted structure graph. For example, when the program fails to resolve two or more quantum dots, the resulting centroid will pollute the final distribution.

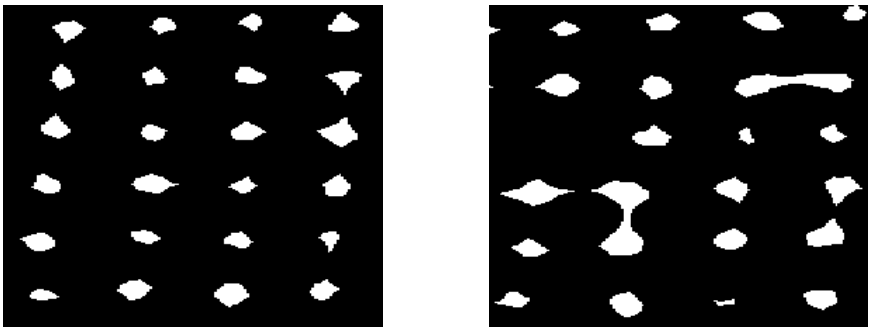

Figure A.8: ***On the left:*** *features are resolved properly and each white region represent a single quantum dot.* ***On the right:*** *features are not properly resolved and some regions are either missing or contains more than one nanoparticle.*

While the centroid extraction will affect both distribution, the extracted structure graph will affect only the angles distribution. Generally, noise introduced by a poorly extracted graph will result in a noisy distribution with broadened peaks.

There also some problems when the number of particles in the image is too large, because the time required to compute the angles will be too large: this is unfortunate, because large number of particles are better, at least from a statistical point of view.

For this last issue, some improvements can be obtain by changing how the generation of the graph works, which is already underway. But for the other issues little can be done, beside obtaining better images.

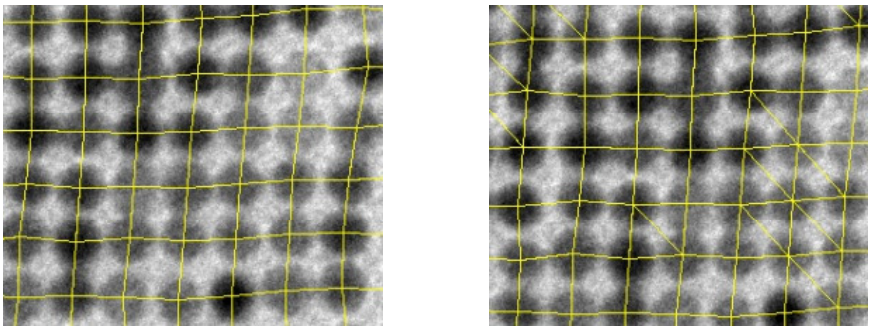

Figure A.9: ***On the left:*** *only the expected 4 neighbours are connected by the graph.* ***On the right:*** *for some quantum dots more than 4 neighbours are connected by the graph, resulting in spurious contribution to the angles distribution.*

Acknowledgements

First of all, I would like to thank prof. Daniël Vanmaekelbergh and dr. Ingmar Swart, who gave me the opportunity to work on this particular topic. To use a technical jargon, it was a bumpy ride: I was warned about all the complexities that were ahead of me when I was about to chose this particular project, but I have made it. I have learned a lot in these two years and I am looking forward to improve on what I have learned thus so far.

I would like to thank my two awesome daily supervisors: Carlo and Jaco. Both taught me everything needed in order to survive in a chemistry lab and more importantly, the love for honeycomb supercrystals and the basics of self-assembly. Thank you Jaco for helping me even while you were busy in Grenoble shooting X-Rays like a true mad scientist, and thank you Carlo for taking his place. I was very lucky to have you both as mentors during this scientifical journey.

Then, well, my stay at CMI would have been the same without the people in there. In the master room, lots of hugs have to be administered. Annalies, for all the candies and the useful discussions about chemistry; Marieke, for having listened through all my non-sense in one year and a half; Maro, who shared the joys and frustrations of PbSe supercrystals; Adrian, who shared his precious hummus with me during the few Harold's lessons that I've attended; Mark, for all the useful discussions about quantum dots, self-assembly and tractor pulling. But I have also to thank all the people that helped me in my path: Joost for all the useful DFT-related discussions, Joep for all the help he gave me in everything related to self-assembly and such and last but not least, to Hans for keeping everything up and running in the lab.

But I was also very lucky to meet lots of awesome people during my stay, and I would like to also thank them. Michele, for all the "Alé paolino" shouted in these last two years and for saving my ass when I was looking for housing in Utrecht; Cinzia, aka 'stella' (emojis, sadly, are not properly rendered in LaTeX yet), for all the times that I needed a person to talk to and, to put it in simple words, for being an awesome friend; Jorgos, for the countless hours spent in Sterk yelling against a particular problem and all the time spent together in the last one year and a half talking about physics, climbing and yelling "Fucking Denia" everytime poor Denia was remarking something useful (or not); Stefano, for being my favourite theoretical physicist, with an awesome taste in books, music and mind bending experiences; Chiara, for all the beers, laughs and discussions about politics, maths and human beings; Adam, for making us feel closer to the scottish indipendence cause and for preparing Haggis the scottish way, including poetry and kilt; George, for sharing a passion for the right kind of music and, well, the feeling of falling in love every five minutes; Daniele, for the countless discussions about chemistry and nanoparticles but, more importantly, for helping me out during my stay at ETH.

Alessio, Bruno, Gaetano, Denia (Fuckin' Denia), Walter aka 'Bomberone', Fabrizio, Monica, Giulia, Matteo, are some of the people that I owe a Thank you for more than one reason. And, finally, to my two special housemates, Peter and Yannos. Thank you guys :)

Last but not least, to the most important ones: to my family. A special thank to my mum, my dad and my brother: without you I would not have been able to do this. You have encouraged me to go abroad and supported all along the way. This experience changed me in many ways and, to put it simple, words can hardly express my graditude.

Bibliography

[1] Celso de Mello Donegá. "Synthesis and properties of colloidal heteronanocrystals". *Chemical Society Reviews* 40, p. 1512, 2011. DOI: 10.1039/c0cs00055h. (Cit. on p. 7).

[2] Joep L. Peters. "Fabrication of single crystalline ultra-thin superlattices by self-assembly via oriented attachment of PbTe nanocrystals" (cit. on pp. 7, 15, 27, 31, 43).

[3] Christopher B. Murray, C. R. Kagan, and M. G. Bawendi. "Synthesis and characterization of monodisperse nanocrystals and close-packed nanocrystal assemblies". *Annual Review of Materials Science* 30, pp. 545–610, 2000. (Cit. on p. 9).

[4] Antti Hassinen, Iwan Moreels, Kim De Nolf, Philippe F. Smet, José C. Martins, and Zeger Hens. "Short-Chain Alcohols Strip X-Type Ligands and Quench the Luminescence of PbSe and CdSe Quantum Dots, Acetonitrile Does Not". *Journal of the American Chemical Society* 134, pp. 20705–20712, 2012. DOI: 10.1021/ja308861d. (Cit. on p. 10).

[5] Marcin Fialkowski, Kyle J. M. Bishop, Rafal Klajn, Stoyan K. Smoukov, Christopher J. Campbell, and Bartosz A. Grzybowski. "Principles and Implementations of Dissipative (Dynamic) Self-Assembly". *The Journal of Physical Chemistry B* 110, pp. 2482–2496, 2006. DOI: 10.1021/jp054153q. (Cit. on p. 12).

[6] Dmitri V. Talapin, Andreas Kornowski, Andrey L. Rogach, Elena V. Shevchenko, Nikolai Gaponik, Markus Haase, and Horst Weller. "A new approach to crystallization of CdSe nanoparticles into ordered three-dimensional superlattices". 2001. (Cit. on pp. 13, 14, 35).

[7] R. Lee Penn and Jillian F. Banfield. "Oriented attachment and growth, twinning, polytypism, and formation of metastable phases: Insights from nanocrystalline TiO2". *American Mineralogist* 83, pp. 1077–1082, 1998. (Cit. on p. 14).

[8] Kyung-Sang Cho, Dmitri V. Talapin, Wolfgang Gaschler, and Christopher B. Murray. "Designing PbSe Nanowires and Nanorings through Oriented Attachment of Nanoparticles". *Journal of the American Chemical Society* 127, pp. 7140–7147, 2005. DOI: 10.1021/ja050107s. (Cit. on pp. 14, 16, 29).

[9] Cleocir José Dalmaschio, Caue Ribeiro, and Edson Roberto Leite. "Impact of the colloidal state on the oriented attachment growth mechanism". *Nanoscale* 2, p. 2336, 2010. DOI: 10.1039/c0nr00338g. (Cit. on p. 15).

[10] E. Kalesaki, C. Delerue, C. Morais Smith, W. Beugeling, G. Allan, and D. Vanmaekelbergh. "Dirac Cones, Topological Edge States, and Nontrivial Flat Bands in Two-Dimensional Semiconductors with a Honeycomb Nanogeometry". *Physical Review X* 4, 2014. DOI: 10.1103/PhysRevX.4.011010. (Cit. on pp. 15, 19).

[11] WIEL H. EVERS, BART GORIS, SARA BALS, MARIANNA CASAVOLA, JOOST DE GRAAF, RENÉ VAN ROIJ, MARJOLEIN DIJKSTRA, and DANIËL VANMAEKELBERGH. "Low-Dimensional Semiconductor Superlattices Formed by Geometric Control over Nanocrystal Attachment". *Nano Letters* 13, pp. 2317–2323, 2013. DOI: 10.1021/n1303322k. (Cit. on pp. 15, 28, 30, 31).

[12] S. A. P. VAN ROSSUM. "Single crystalline PbS thin films via oriented attachment" (cit. on p. 15).

[13] DMITRI V. TALAPIN, ELENA V. SHEVCHENKO, CHRISTOPHER B. MURRAY, ALEXEY V. TITOV, and PETR KRÁL. "Dipole=Dipole Interactions in Nanoparticle Superlattices". *Nano Letters* 7, pp. 1213–1219, 2007. DOI: 10.1021/n1070058c. (Cit. on pp. 16, 30).

[14] MARK KLOKKENBURG, ARJAN J. HOUTEPEN, ROLF KOOLE, JULIUS W. J. DE FOLTER, BEN H. ERNÉ, ERNST VAN FAASSEN, and DANIËL VANMAEKELBERGH. "Dipolar Structures in Colloidal Dispersions of PbSe and CdSe Quantum Dots". *Nano Letters* 7, pp. 2931–2936, 2007. DOI: 10.1021/n10714684. (Cit. on p. 16).

[15] TOBIAS HANRATH. "Colloidal nanocrystal quantum dot assemblies as artificial solids". *Journal of Vacuum Science & Technology A: Vacuum, Surfaces, and Films* 30, p. 030802, 2012. DOI: 10.1116/1.4705402. (Cit. on p. 17).

[16] AMIR ZABET-KHOSOUSI and AL-AMIN DHIRANI. "Charge Transport in Nanoparticle Assemblies". *Chemical Reviews* 108, pp. 4072–4124, 2008. DOI: 10.1021/cr0680134. (Cit. on p. 17).

[17] D. L. NIKA, E. P. POKATILOV, Q. SHAO, and A. A. BALANDIN. "Charge-carrier states and light absorption in ordered quantum dot superlattices". *Physical Review B* 76, 2007. DOI: 10.1103/PhysRevB.76.125417. (Cit. on p. 18).

[18] OLGA L. LAZARENKOVA and ALEXANDER A. BALANDIN. "Miniband formation in a quantum dot crystal". *Journal of Applied Physics* 89, p. 5509, 2001. DOI: 10.1063/1.1366662. (Cit. on p. 18).

[19] PHILIP W. ANDERSON. "Absence of diffusion in certain random lattices". *Physical review* 109, p. 1492, 1958. (Cit. on p. 18).

[20] C. B. MURRAY, C. R. KAGAN, and M. G. BAWENDI. "Self-organization of CdSe nanocrystallites into three-dimensional quantum dot superlattices". *Science* 270, pp. 1335–1338, 1995. (Cit. on pp. 18, 35).

[21] M. V. ARTEMYEV, A. I. BIBIK, L. I. GURINOVICH, S. V. GAPONENKO, and U. WOGGON. "Evolution from individual to collective electron states in a dense quantum dot ensemble". *Physical Review B* 60, p. 1504, 1999. (Cit. on pp. 18, 35).

[22] E. KALESAKI, W. H. EVERS, G. ALLAN, D. VANMAEKELBERGH, and C. DELERUE. "Electronic structure of atomically coherent square semiconductor superlattices with dimensionality below two". *Physical Review B* 88, 2013. DOI: 10.1103/PhysRevB.88.115431. (Cit. on p. 19).

[23] ERNESTO O. WRASSE and TOME M. SCHMIDT. "Prediction of Two-Dimensional Topological Crystalline Insulator in PbSe Monolayer". *Nano Letters* 14, pp. 5717–5720, 2014. DOI: 10.1021/n1502481f. (Cit. on p. 19).

[24] W. Beugeling, E. Kalesaki, C. Delerue, Y.-M. Niquet, D. Vanmaekelbergh, and C. Morais Smith. "Topological states in multi-orbital HgTe honeycomb lattices". *Nature Communications* 6, p. 6316, 2015. doi: 10.1038/ncomms7316. (Cit. on p. 19).

[25] Sungwoo Kim, Jaehong Noh, Hyekyoung Choi, Heonseok Ha, Jung Hoon Song, Hyung Cheoul Shim, Jihoon Jang, Matthew C. Beard, and Sohee Jeong. "One-Step Deposition of Photovoltaic Layers Using Iodide Terminated PbS Quantum Dots". *The Journal of Physical Chemistry Letters* 5, pp. 4002–4007, 2014. doi: 10.1021/jz502092x. (Cit. on pp. 20, 25, 36).

[26] Ju Young Woo, Jae-Hyeon Ko, Jung Hoon Song, Kyungnam Kim, Hyekyoung Choi, Yong-Hyun Kim, Doh C. Lee, and Sohee Jeong. "Ultrastable PbSe Nanocrystal Quantum Dots via *in Situ* Formation of Atomically Thin Halide Adlayers on PbSe(100)". *Journal of the American Chemical Society* 136, pp. 8883–8886, 2014. doi: 10.1021/ja503957r. (Cit. on pp. 20, 21, 34, 37).

[27] Hyekyoung Choi, Jae-Hyeon Ko, Yong-Hyun Kim, and Sohee Jeong. "Steric-Hindrance-Driven Shape Transition in PbS Quantum Dots: Understanding Size-Dependent Stability". *Journal of the American Chemical Society* 135, pp. 5278–5281, 2013. doi: 10.1021/ja400948t. (Cit. on p. 20).

[28] Iwan Moreels, Bernd Fritzinger, José C. Martins, and Zeger Hens. "Surface Chemistry of Colloidal PbSe Nanocrystals". *Journal of the American Chemical Society* 130, pp. 15081–15086, 2008. doi: 10.1021/ja803994m. (Cit. on p. 20).

[29] Kenrick J. Williams, William A. Tisdale, Kurtis S. Leschkies, Greg Haugstad, David J. Norris, Eray S. Aydil, and X.-Y. Zhu. "Strong Electronic Coupling in Two-Dimensional Assemblies of Colloidal PbSe Quantum Dots". *ACS Nano* 3, pp. 1532–1538, 2009. doi: 10.1021/nn9001819. (Cit. on p. 21).

[30] C. S. Suchand Sandeep, Jon Mikel Azpiroz, Wiel H. Evers, Simon C. Boehme, Iwan Moreels, Sachin Kinge, Laurens D. A. Siebbeles, Ivan Infante, and Arjan J. Houtepen. "Epitaxially Connected PbSe Quantum-Dot Films: Controlled Neck Formation and Optoelectronic Properties". *ACS Nano* 8, pp. 11499–11511, 2014. doi: 10.1021/nn504679k. (Cit. on p. 21).

[31] Arjan J. Houtepen, Rolf Koole, Daniël Vanmaekelbergh, Johannes Meeldijk, and Stephen G. Hickey. "The Hidden Role of Acetate in the PbSe Nanocrystal Synthesis". *Journal of the American Chemical Society* 128, pp. 6792–6793, 2006. doi: 10.1021/ja061644v. (Cit. on p. 23).

[32] M. P. Boneschanscher, W. H. Evers, J. J. Geuchies, T. Altantzis, B. Goris, F. T. Rabouw, S. A. P. van Rossum, H. S. J. van der Zant, L. D. A. Siebbeles, G. Van Tendeloo, I. Swart, J. Hilhorst, A. V. Petukhov, S. Bals, and D. Vanmaekelbergh. "Long-range orientation and atomic attachment of nanocrystals in 2D honeycomb superlattices". *Science* 344, pp. 1377–1380, 2014. doi: 10.1126/science.1252642. (Cit. on pp. 23, 30).

[33] Jiang Tang, Kyle W. Kemp, Sjoerd Hoogland, Kwang S. Jeong, Huan Liu, Larissa Levina, Melissa Furukawa, Xihua Wang, Ratan Debnath, Dongkyu Cha, et al. "Colloidal-quantum-dot photovoltaics using atomic-ligand passivation". *Nature materials* 10, pp. 765–771, 2011. (Cit. on pp. 24, 36, 38, 41, 42).

[34] ANGANG DONG, YUCONG JIAO, and DELIA J. MILLIRON. "Electronically Coupled Nanocrystal Superlattice Films by *in Situ* Ligand Exchange at the Liquid–Air Interface". *ACS Nano* 7, pp. 10978–10984, 2013. DOI: 10.1021/nn404566b. (Cit. on p. 24).

[35] SANDRINE ITHURRIA and DMITRI V. TALAPIN. "Colloidal Atomic Layer Deposition (c-ALD) using Self-Limiting Reactions at Nanocrystal Surface Coupled to Phase Transfer between Polar and Nonpolar Media". *Journal of the American Chemical Society* 134, pp. 18585–18590, 2012. DOI: 10.1021/ja308088d. (Cit. on p. 26).

[36] GUANGDA NIU, LIDUO WANG, RUI GAO, WENZHE LI, XUDONG GUO, HAOPENG DONG, and YONG QIU. "Inorganic halogen ligands in quantum dots: I=, Br=, Cl= and film fabrication through electrophoretic deposition". *Physical Chemistry Chemical Physics* 15, p. 19595, 2013. DOI: 10.1039/c3cp52678j. (Cit. on p. 25).

[37] HAO ZHANG, JAEYOUNG JANG, WENYONG LIU, and DMITRI V. TALAPIN. "Colloidal Nanocrystals with Inorganic Halide, Pseudohalide, and Halometallate Ligands". *ACS Nano* 8, pp. 7359–7369, 2014. DOI: 10.1021/nn502470v. (Cit. on pp. 25, 36).

[38] ANGSHUMAN NAG, HAO ZHANG, ERIC JANKE, and DMITRI V. TALAPIN. "Inorganic Surface Ligands for Colloidal Nanomaterials". *Zeitschrift für Physikalische Chemie* 229, 2015. DOI: 10.1515/zpch-2014-0604. (Cit. on p. 25).

[39] IWAN MOREELS, KAREL LAMBERT, DAVID DE MUYNCK, FRANK VANHAECKE, DIRK POELMAN, JOSÉ C. MARTINS, GUY ALLAN, and ZEGER HENS. "Composition and Size-Dependent Extinction Coefficient of Colloidal PbSe Quantum Dots". *Chemistry of Materials* 19, pp. 6101–6106, 2007. DOI: 10.1021/cm071410q. (Cit. on p. 27).

[40] J. J. GEUCHIES. "Atomically choerent nanocrystals superlattices" (cit. on pp. 27, 31, 36, 44).

[41] CHANGMING FANG, MARIJN A. VAN HUIS, DANIËL VANMAEKELBERGH, and HENNY W. ZANDBERGEN. "Energetics of Polar and Nonpolar Facets of PbSe Nanocrystals from Theory and Experiment". *ACS Nano* 4, pp. 211–218, 2010. DOI: 10.1021/nn9013406. (Cit. on p. 28).

[42] R. J. KORTSCHOT, J. VAN RIJSSEL, R. J. A. VAN DIJK-MOES, and B. H. ERNÉ. "Equilibrium Structures of PbSe and CdSe Colloidal Quantum Dots Detected by Dielectric Spectroscopy". *The Journal of Physical Chemistry C* 118, pp. 7185–7194, 2014. DOI: 10.1021/jp412389e. (Cit. on p. 29).

[43] WILLIAM J. BAUMGARDNER, KEVIN WHITHAM, and TOBIAS HANRATH. "Confined-but-Connected Quantum Solids via Controlled Ligand Displacement". *Nano Letters* 13, pp. 3225–3231, 2013. DOI: 10.1021/nl401298s. (Cit. on p. 32).

[44] MILAN SYKORA, ALEXEY Y. KOPOSOV, JOHN A. MCGUIRE, ROLAND K. SCHULZE, OLEXANDR TRETIAK, JEFFREY M. PIETRYGA, and VICTOR I. KLIMOV. "Effect of Air Exposure on Surface Properties, Electronic Structure, and Carrier Relaxation in PbSe Nanocrystals". *ACS Nano* 4, pp. 2021–2034, 2010. DOI: 10.1021/nn100131w. (Cit. on p. 34).

[45] EVELYN L. ROSEN, RAFFAELLA BUONSANTI, ANNA LLORDES, APRIL M. SAWVEL, DELIA J. MILLIRON, and BRETT A. HELMS. "Exceptionally Mild Reactive Stripping of Native Ligands from Nanocrystal Surfaces by Using Meerwein's Salt". *Angewandte Chemie International Edition* 51, pp. 684–689, 2012. DOI: 10.1002/anie.201105996. (Cit. on p. 36).

[46] C. H. HENRY. "Limiting efficiencies of ideal single and multiple energy gap terrestrial solar cells". *Journal of Applied Physics* 51, p. 4494, 1980. DOI: 10.1063/1.328272. (Cit. on p. 36).

[47] ANGSHUMAN NAG, MAKSYM V. KOVALENKO, JONG-SOO LEE, WENYONG LIU, BORIS SPOKOYNY, and DMITRI V. TALAPIN. "Metal-free Inorganic Ligands for Colloidal Nanocrystals: S^{2-}, HS^{-}, Se^{2-}, HSe^{-}, Te^{2-}, HTe^{-}, TeS_3^{2-}, OH^{-}, and NH_2^{-} as Surface Ligands". *Journal of the American Chemical Society* 133, pp. 10612–10620, 2011. DOI: 10.1021/ja2029415. (Cit. on p. 36).

[48] JING HUANG, WENYONG LIU, DMITRIY S. DOLZHNIKOV, LOREDANA PROTESESCU, MAKSYM V. KOVALENKO, BONIL KOO, SOMA CHATTOPADHYAY, ELENA V. SHENCHENKO, and DMITRI V. TALAPIN. "Surface Functionalization of Semiconductor and Oxide Nanocrystals with Small Inorganic Oxoanions (PO_4^{3-}, MoO_4^{2-}) and Polyoxometalate Ligands". *ACS Nano* 8, pp. 9388–9402, 2014. DOI: 10.1021/nn503458y. (Cit. on p. 36).

[49] ANGANG DONG, JUN CHEN, PATRICK M. VORA, JAMES M. KIKKAWA, and CHRISTOPHER B. MURRAY. "Binary nanocrystal superlattice membranes self-assembled at the liquid–air interface". *Nature* 466, pp. 474–477, 2010. DOI: 10.1038/nature09188. (Cit. on p. 39).